An Evaluation of Microwave Land Surface Emissivities Over the Continental United States to Benefit GPM-Era Precipitation Algorithms

Ralph R. Ferraro, Christa D. Peters-Lidard, Cecilia Hernandez, F. Joseph Turk, Filipe Aires, Catherine Prigent, Xin Lin, Sid-Ahmed Boukabara, Fumie A. Furuzawa, Kaushik Gopalan, Kenneth W. Harrison, Fatima Karbou, Li Li, *Senior Member, IEEE*, Chuntao Liu, Hirohiko Masunaga, Leslie Moy, Sarah Ringerud, Gail M. Skofronick-Jackson, Yudong Tian, and Nai-Yu Wang

Abstract—Passive microwave (PMW) satellite-based precipitation over land algorithms rely on physical models to define the most appropriate channel combinations to use in the retrieval, yet typically require considerable empirical adaptation of the model for use with the satellite measurements. Although low-frequency channels are better suited to measure the emission due to liquid associated with rain, most techniques to date rely on high-frequency, scattering-based schemes since the low-frequency methods are limited to the highly variable land surface background, whose radiometric contribution is substantial and can vary more than the contribution of the rain signal. Thus, emission techniques are generally useless over the majority of the Earth's surface. As a first step toward advancing to globally useful physical retrieval schemes, an intercomparison project was organized to determine the accuracy and variability of several emissivity retrieval schemes. A three-year period (July 2004–June 2007) over different targets with varying surface characteristics was developed. The PMW radiometer data used includes the Special Sensor Microwave Imagers, SSMI Sounder, Advanced Microwave Scanning Radiometer (AMSR-E), Tropical Rainfall Measuring Mission (TRMM) Microwave Imager (TMI), Advanced Microwave Sounding Units, and Microwave Humidity Sounder, along with land surface model emissivity estimates. Results from three specific targets in North America were examined. While there are notable discrepancies among the estimates, similar seasonal trends and associated variability were noted. Because of differences in the treatment surface temperature in the various techniques, it was found that comparing the product of temperature and emissivity yielded more insight than when comparing the emissivity alone. This product is the major contribution to the overall signal measured by PMW sensors and, if it can be properly retrieved, will improve the utility of emission techniques for over land precipitation retrievals. As a more rigorous means of comparison, these emissivity time series were analyzed jointly with precipitation data sets, to examine the emissivity response immediately following rain events. The results demonstrate that while the emissivity structure can be fairly well characterized for certain surface types, there are other more complex surfaces where the underlying variability is more than can be captured with the PMW channels. The implications for Global Precipitation Measurement-era algorithms suggest that physical retrievals are feasible over vegetated land during the warm seasons.

Index Terms—Emissivity, land surface, passive microwave remote sensing, precipitation.

R. R. Ferraro is with NOAA/NESDIS, College Park, MD 20740 USA (e-mail: Ralph.R.Ferraro@noaa.gov).

C. D. Peters-Lidard, G. M. Skofronick-Jackson, and Y. Tian are with the NASA Goddard Space Flight Center, Greenbelt, MD 20771 USA.

C. Hernandez is with the University of Maryland, College Park, MD 20740 USA.

F. J. Turk is with the Radar Science Group, Jet Propulsion Laboratory, Pasadena, CA 91109 USA.

F. Aires is with Estellus, Paris, France.

C. Prigent is with the Laboratoire d'Etudes du Rayonnement et de la Matière en Astrophysique, Paris Observatory, Centre National de la Recherche Scientifique, Paris, France.

X. Lin is with the Earth System Science Interdisciplinary Center, University of Maryland, College Park, MD 20740 USA, and also with the NASA Goddard Space Flight Center, Greenbelt, MD 20771 USA.

S.-A. Boukabara and L. Moy are with the NOAA/NESDIS, Camp Springs, MD 20746 USA.

F. A. Furuzawa and H. Masunaga are with the Hydrospheric Atmospheric Research Center, Nagoya University, Nagoya, Japan.

K. Gopalan is with the Space Applications Center, Ahmedabad, India.

K. W. Harrison is with North Carolina State University, Raleigh, NC 27695 USA.

F. Karbou is with the National Centre for Meteorological Research/GAME, Toulouse, France.

L. Li is with the Naval Research Laboratory, Washington, DC 20375 USA.

C. Liu is with the Department of Atmospheric Sciences, University of Utah, Salt Lake City, UT 84112 USA.

S. Ringerud is with the Colorado State University, Boulder, CO 80309 USA.

N.-Y. Wang is with the Earth System Science Interdisciplinary Center, University of Maryland, College Park, MD 20740 USA.

I. INTRODUCTION

THE derivation of microwave surface emissivity from low earth orbiting satellite-based passive microwave (PMW) radiometers begins with the proper characterization of the surface geophysical state. In general, lower surface emissivity is correlated with increasing soil moisture. PMW techniques for estimating soil moisture at L-band (1–2 GHz) are based on the contrast between the dielectric constant of liquid water (near 80) and dry soil (between 2 and 4 depending upon soil type). The dielectric constant of the soil-water mixture increases with increasing moisture, lowering the surface emissivity with a corresponding decrease in the observed brightness temperature (TB) [1]. For over-land PMW precipitation algorithms, the surface emissivity forms the background for the top of atmosphere radiance measured by a satellite-based radiometer. An improved characterization of the land surface will be crucial to
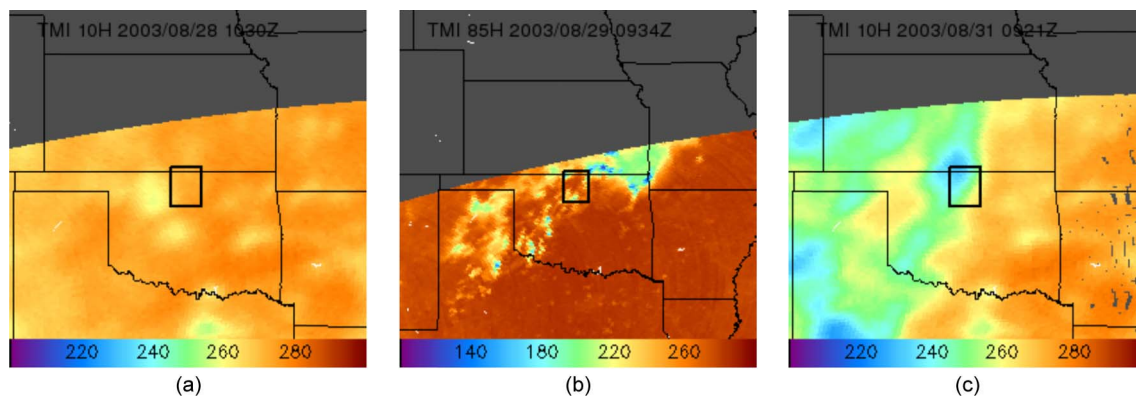
Fig. 1.   Change in the TMI 10 GHz T_B (Kelvin scale) over the southern United States due to series of rain events that moved across the are between 29 and 30 August 2003. (a) 10H GHz T_B prior to the rain event, at 1030 UTC on 28 August. (b) TMI 85H T_B at 0943 UTC on 29 August, indicating the movement of convective-based precipitation across the area. (c) 10H GHz T_B two days later at 0921 UTC on 31 August, after the rain systems had passed though. The small box in each image indicates a 1-degree box centered in the domain of the Southern Great Plains (SGP) site ($36.6°$ N $97.5°$ W).

better exploit the observations that will be gathered from the joint National Aeronautics and Space Administration (NASA) and the Japanese Aerospace Exploration Agency (JAXA) Global Precipitation Measurement (GPM) Mission instruments. Unlike its predecessor, the Tropical Rainfall Measuring Mission (TRMM) satellite, the core GPM satellite will orbit at a higher inclination ($65°$ compared to $35°$ for TRMM), providing more observations of land areas whose coverage is subject to wider seasonal variations such as snow cover, seasonal crop lands, forests, partially frozen lakes at higher latitudes, to irrigated lands, deserts and tropical rainforests closer to the equator. The GPM Microwave Imager (GMI) includes high-frequency (HF) channels at 166 GHz and at 190 GHz, which are common to many microwave sounding radiometers, and will be important for detecting cold season precipitation.

Of particular relevance to this effort are satellite-based observations gathered from the suite of conically scanning PMW radiometers orbiting on low earth satellites and making observations in the frequency range from 10 to 190 GHz, since these sensors will complement the core GPM satellite observations. In addition to TRMM, this includes the long running (1987–current) system of Special Sensor Microwave Imagers (SSMI) and its follow-on, the SSMI Sounder (SSMIS), and the WindSat polarimetric radiometer onboard the Coriolis satellite. These observations are augmented with PMW sounder observations from the Advanced Microwave Sounding Units (AMSU) onboard the National Oceanic and Atmospheric Administration (NOAA) and EUMETSAT MetOp satellites, in particular the AMSU-B and Microwave Humidity Sounder (MHS) instruments. AMSR-E has also made contributions to the constellation, but has recently stopped operating in 2011.

While considerable progress has been made in characterizing the uncertainty in the over-ocean precipitation estimates from these sensors, the over-land estimates have improved only marginally [2], [3]. Present day over-land PMW precipitation algorithms can generally be classified as semi-empirical; they use physically developed models to define the most important satellite channel combinations for precipitation detection and precipitation rates, but then often employ statistical techniques to identify regions of precipitation and its intensity. Often the highly variable land surface background and its associated

emissivity can contribute more uncertainty to the precipitation estimate than the contribution due the rain signal itself. In practice, there is considerable empirical tuning and adaptation of these models for use with the variety of satellite/sensor observations. However, if the characteristics of the land surface background can be determined, then more physically based retrieval techniques (e.g., emission-based due to liquid clouds and rain; scattering-based due to precipitation-sized frozen hydrometeors) can be utilized.

There is a natural correspondence between soil moisture and precipitation. Soil moisture controls the partitioning of precipitation into infiltration, surface runoff, and evaporation/transpiration from land surfaces. Immediately following rainfall events, a strong correspondence should exist between the spatial distribution of emissivity and precipitation if the ground is not close to saturation. The precipitation time history modulates the surface emissivity [4]. If it is raining during a satellite overpass, the surface rainfall quickly alters the surface and its emissivity; depending upon the revisit interval of the subsequent satellite overpass, the emissivity changes further as the surface dries out and the water is absorbed by surface vegetation. As an example, Fig. 1 shows the depression in the 10 GHz TB surrounding the Southern Great Plains (SGP) site near the Kansas–Oklahoma border due to increased soil moisture following a rain event (Fig. 1(a) = 10 GHz before rain, Fig. 1(b) = 85 GHz during rain, Fig. 1(c) = 10 GHz after rain). 10 GHz is the lowest frequency channel (and hence the once most sensitive to surface conditions) found on the TMI and GMI. Therefore, comparisons of surface emissivity retrievals together with the previous-time precipitation totals are an indirect yet qualitative way to validate emissivity retrievals over rain-affected surfaces.

As a first step toward advancing to globally useful physical retrieval schemes, an intercomparison project was organized under the auspices of the NASA Precipitation Measurement Missions (PMM) science team to determine the accuracy and variability of several mature and emerging emissivity retrieval schemes. Many of these emissivity data sets were derived under nonprecipitating (cloud-free) conditions, developed for use in numerical weather prediction (NWP) data assimilation. In general, these tend to be for AMSU-A temperature sounding

channels within the 50–60 GHz oxygen rotational line complex, whereas the GPM era precipitation algorithms need to adapt to observations from both window and HF sounding channels. Therefore, this study focuses on a three-year period (July 2004– June 2007) over different targets with varying surface characteristics (e.g., dense vegetation, arid land, agriculture land, snow cover), where common PMW radiometer data were collected, and daily emissivity estimates were produced by each participant. In addition to these subsetted satellite data, ancillary data sets were provided, including model analyses from the National Centers for Environmental Prediction (NCEP) and cloud information from the International Satellite Cloud Climatology Project (ISCCP) [5], which are needed by many of the techniques and also for land surface model-(LSM) driven emissivity estimates.

The emissivity estimates presented here are largely representative of nonprecipitating scenes. However, for a complete characterization of the varying surface emissivity input to GPM core algorithms, it is important to know how the emissivity varies owing to the presence or recent occurrence of precipitation. Onset of rain can modify the top level soil moisture [6] and associated emissivity [1] on the scale of minutes, and retains a memory even after the rainfall ceases. The extent of this precipitation/surface coupling exhibits a high spatial and temporal variability, such that knowledge of the surface properties at one time may not be very useful at some future time. One way to adapt is to carry over information from one satellite overpass to the next via a dynamic emissivity database that incorporates the history of the antecedent precipitation. On the other hand, since LSMs are driven with precipitation observations, they physically adapt to changing weather conditions and modify surface properties, which can subsequently be fed to radiative transfer models (RTMs) to consistently estimate surface emissivities at multiple channels. Since the land emissivities at window channels between 19 and 85 GHz are highly correlated, data reduction techniques are useful to extract independent information and classify self-similar surfaces. For example, scenes containing coastlines are so variable that surface-sensitive channels may never be useful. Over the $\pm 65°$ latitudes over which the GPM-core will cover, these questions are ill-posed and in need of further analysis.

In order to assess the current status of established and emerging emissivity data sets and techniques, the PMM Land Surface Characterization Working Group (LSWG), a group of approximately 25 principal investigators *et al.* devised a study whereby each participant would contribute emissivity estimates generated over common targets with varying surface characteristics and compared over different time scales (e.g., instantaneous and monthly). In this paper, we focus on the results from three specific targets of the study where a high confidence in understanding the seasonal and interannual surface characteristics exists. While limited, this study represents the first intercomparison specifically focused upon studying the applicability of several different approaches for estimation of microwave surface emissivity. These sites include the U.S. SGP; the NOAA Hydrometeorological Testbed (HMT) Southeast U.S. site (HMT-SE), and the Canadian CloudSat CALIPSO Validation Program (C3VP) site in southern Ontario, Canada.

Each investigator was provided common input data sets and encouraged to use them (although some groups already have mature products independent of this study) and was responsible for providing an associated emissivity product and land surface temperature, at the spatial and time scale of their particular method. After a brief discussion of each technique, the various analysis techniques are presented for each site. Suggestions for further studies to establish a more complete description of the global surface emissivity for the GPM algorithms are provided.

II. DESCRIPTION OF THE STUDY

The goal of the LSWG study was to examine similarities and differences of the various methodologies and assess potential impacts of these differences on PMW-based precipitation retrievals. For example, if there is relatively good agreement over "stable" targets like lightly vegetated land, then perhaps these surfaces would be appropriate for an initial focus of the physical algorithm development.

More specifically, an initial data period of one year was expanded to three years (July 2004–June 2007) to give more robustness to the results (although not all investigators were able to expand their retrievals to the longer time period). Twelve targets were selected, some which were common with activities well underway by the International TIROS Operational Vertical Sounder Working Group that included open ocean (three sites), inland water, wetland surface, rain forest (two sites), high latitude land (two sites), desert, and continental/agricultural land (two sites). As mentioned above, this paper focuses on the results from three sites: SGP (centered at 35N 97W); HMT-SE (34N 81W); and C3VP (44N 80W). All have seasonal changes in vegetation cover, although the type of vegetation varies. They are all subject to winter snowfall, with C3VP receiving the most snowfall. Other similarities and differences will be further discussed in Section IV.

Several data sets were assembled to assist with the emissivity generation and their evaluation. Each investigator was to use, where possible, common data sets assembled by the LSWG (however, mature data sets which were already developed were not restricted to the common data). For the satellite data, AMSR-E, SSMI, SSMIS, TMI, WindSat and AMSU/MHS TB's were prepared within a 1-degree latitude/longitude grid centered at the above target coordinates. In addition to the satellite TB's, ancillary data from the NCEP Global Data Assimilation System (GDAS) model (e.g., surface temperature, vertical temperature and moisture profiles, precipitation, radiation, wind speed), LDAS surface parameters, TRMM PR and VIRS data, ISCCP cloud mask and 3-hourly rainfall estimates from the Climate Prediction Center's Morphing Technique (CMORPH), TRMM Multisatellite Precipitation Analysis (TRMM 3B42 product), and the Naval Research Laboratory (NRL)-Blend [7]–[9]. These high-time resolution precipitation data provide the previous time precipitation history for a time interval prior to a satellite overpass. Such precipitation history information is useful to stratify the results under clear, cloudy, and raining conditions. All data were made available to participants through a study web site.

TABLE I
SUMMARY OF EMISSIVITY INTERCOMPARISON PARTICIPANT GROUPS AND DATA SET ATTRIBUTES

Algorithm Group	Sensor	Targets	Dates	Channels
NASA- GSFC	AMSR-E	All	07/04 - 06/07	All
	SSMI	All	07/04 - 06/07	All
	TMI	SGP, HMT-SE	07/04 - 06/07	All
CNRS	SSMI	All	07/04 – 06/07	All
Meteo-France	AMSU-A	All	07/06 - 06/07	23.8; 31.4; 50.3; 89 GHz
	SSMI	All	07/06 - 06/07	All
NOAA-CICS	AMSU-B/MHS	C3VP	12/05 - 02/07	All
Nagoya University	TMI	SGP, HMT-SE	07/04 - 06/07	All
NOAA-MIRS	AMSR-E	All	08/05 - 06/07	All
	AMSU-A, AMSU-B/MHS	All	08/05 - 06/07	All – AMSU (A & B)
	SSMIS	All	08/05 - 06/07	All
NRL/JPL	WindSat	All	07/04 - 06/07	All

TABLE II
DISTINCTION BETWEEN THE THREE MAIN APPROACHES TO MICROWAVE SURFACE EMISSIVITY ESTIMATION USED IN THIS INTERCOMPARISON STUDY

Type	Principle	Input Parameters	Advantages	Disadvantages
Land Surface Model	Dense media radiative transfer theory	Surface parameters (soil type, snow properties, etc)	Naturally couples to land surface models	Dependent upon realism of specified surface parameters
Direct observational	Observationally based	Satellite observations, land and atmosphere properties	No surface parameters needed other than temperature	Only works for partially-opaque atmospheric conditions, dependent upon land surface temperature and atmospheric profile and atmospheric model assumptions
Physical Retrieval	Parameterized radiative transfer	Satellite observations	Physical consistency amongst retrieved surface parameters	Parameterizations may not work well above X-band

Each participant supplied emissivity estimates and land surface temperature for some or all of the targets, and some or all of the sensors and their associated frequencies. These are summarized in Table I. Of these approaches, they can be roughly categorized into three general types, which are differentiated in Table II. The first, observationally based, offers the simplest approach where the effective surface emissivity is directly retrieved from clear scene satellite observations, provided the atmospheric transmissivity and land surface temperature is known (e.g., CNRS). These methods are described in Section III-A. The second method is via rigorous solution to dense media microwave radiative transfer theory, when fed with surface properties such as soil type, snow grain size, etc. (e.g., LSM; see Section III-B). Since this method is based upon a forward RTM, it can be adapted into NWP data assimilation systems and LSMs. The third method is via a physical retrieval, where bulk media properties including surface roughness are parameterized (e.g., NRL—see Section III-C). Physical retrievals form the basis for routine soil moisture products from AMSR-E and WindSat [1], [4]. Some of the techniques are hybrids of these approaches [e.g., the Microwave Integrated Retrieval System (MIRS)], which treats the emissivity as an additional parameter in the retrieval. MIRS is also described within Section III-C.

III. DESCRIPTION OF THE EMISSIVITY ESTIMATION METHODS

In this paper, a total of seven different emissivity estimates were received for the intercomparison study, dependent upon sensor and target (summarized in Table I). They include model calculations, direct estimation from satellite observations, and emissivity estimates as part of physical retrieval using satellite observations. A short summary of each method is provided below. The notation used to identify each algorithm in the remaining discussion is shown in parenthesis in the upcoming subsections.

A. Emissivity Estimates Directly From Satellite Observations

In approximate form, neglecting scattering affects, the satellite measurement, or TB, at a particular frequency, ν, and polarization, p, can be written as

$$TB_{\nu,\text{p}} = T_\text{u} + \tau_\nu \left[\varepsilon_{\nu,\text{p}} T_\text{s} + (1 - \varepsilon_{\nu,\text{p}}) T_\text{d} \right] \qquad (1)$$

where T_u is the upwelling atmospheric emission, τ is the atmospheric transmittance, T_s is the surface temperature, $\varepsilon_{\nu,p}$ is the emissivity, and T_d is the downwelling atmospheric emission. Unlike the infrared (IR) where clouds and surfaces can be well-approximated as a blackbody ($\varepsilon \sim 1$), surfaces at MW wavelengths generally scatter a portion of the incident radiation. Over the range of frequencies that will be contained on GPM-era sensors (e.g., 6–190 GHz), the associated emissivity can vary widely and exhibit strong nonlinear characteristics over frequency and polarization [10], [11]. The variations are also a function of surface type [12], [13], [30]. Information on T_s, T_d, and T_u can either be inferred from the satellite measurements themselves or obtained through ancillary data sources and calculated through RTMs. To a first-order approximation, where the atmospheric contribution is neglected, (1) can be simplified to

$$ TB_{\nu,p} = \varepsilon_{\nu,p} T_s. \tag{1a} $$

Thus, gaining an understanding on how the product of these two terms can vary among different estimation techniques can yield insight as to under which land surface conditions, frequencies and polarizations where advancement in physical precipitation algorithms can be achieved. This concept will be explained further in Section IV.

The emissivity can explicitly be calculated from the satellite observations through

$$ \varepsilon_{\nu,p} = \frac{(TB_{\nu,p} - T_u - \tau_\nu T_d)}{[\tau_\nu (T_s - T_d)]} \tag{2} $$

and estimated via

$$ \varepsilon_{\nu,p} = \frac{TB_{\nu,p}}{T_s}. \tag{2a} $$

This methodology has been used by different groups, and four estimates of this kind are compared here [11], [14], [15]. The results differ primarily in the ancillary inputs used in the calculation (surface skin temperature, temperature and water vapor atmospheric profiles, cloud flag), and, to a lesser extent in the radiative transfer code used to estimate T_d and T_u.

National Center for Scientific Research (CNRS): Microwave emissivities of land surfaces under clear conditions are estimated from SSM/I observations by removing contributions from the atmosphere, clouds, and rain using ancillary data from ISCCP and NCEP analyses [16]. The method initially described in [18] calculates the emissivity directly from (2). Cloud-free SSM/I observations are first identified using collocated visible/ IR satellite observations from ISCCP data. The cloud-free atmospheric contribution is then calculated from an estimate of the local atmospheric temperature and humidity profile from NCEP reanalysis. The atmospheric contribution varies spatially and reaches 15% and 50% in the Tropics for 19 and 85 GHz, respectively. Finally, with the surface skin temperature derived from IR observations (ISCCP estimate), the surface emissivity is calculated for all seven SSM/I channels. Emissivity values are calculated with a spatial resolution of 0.25° at the equator, for the 1993–2008 period, for all available SSM/I instruments. Following the methodology described in [17], cloudy microwave emissivities have been estimated from SSM/I obser-

vations, along with the retrieval of surface skin temperature and integrated water vapor and liquid water content. In addition, a parameterization of the frequency, angular, and polarization dependence of the emissivities has been derived from the analysis of SSM/I, AMSU, and TMI retrieved emissivities [17]. This scheme is also utilized with the widely used Radiative Transfer for TIROS Operational Vertical Sounder (RTTOV) [18].

Meteo-France (MF): As part of MF's efforts, emissivity is calculated following (2). Assumptions are made that the surfaces are flat and specular [15]; however, it should be noted for nadir viewing sensors like AMSU and MHS, a Lambertian component can improve the estimates by up to 1% over complex surfaces like snow and desert sand [19]–[21] but is not employed for this intercomparison study. Temperature and humidity profiles from GDAS have been used as input to the RTTOV model to compute the atmospheric contribution to the measured radiances. The goal of the MF emissivity retrievals is for NWP model data assimilation, thus, to ensure that the forward RTM calculations are consistent with satellite observations, and to minimize the rejection of a large amount of data, a land surface emissivity parameterization is used in order to describe the emissivity for AMSU observations. A dynamical retrieval of the emissivity, at two well-selected window channels, is performed to describe the emissivity for temperature and humidity sounding channels [19], [22]–[24]. In addition, feasibility studies have been conducted to extend to the use of SSM/I data and to provide appropriate responses to cloud/rain detection and to the bias correction over land surfaces [25].

NOAA/Cooperative Institute for Climate and Satellites (CICS): As presented in (1), the microwave emission characteristics of a land surface viewed by a satellite microwave radiometer may be inferred by canceling the atmospheric contribution within the observed TB, which can be estimated using RTM calculations assuming clear-sky (cloud-free) conditions. Environmental parameters from the NCEP GDAS model are used as inputs to the RTM. The emissivity is then computed from (2).

In the CICS retrievals, the RTM is utilized on an atmosphere consisting of 100 homogenous layers of 200 m from the surface to the top of the atmosphere. The RTM uses the model of Rosenkranz for water vapor, oxygen, and nitrogen absorption in the atmosphere [26]. The environmental inputs to the RTM from GDAS include the atmospheric profiles of pressure, temperature, and water vapor at 21 levels as well as the surface temperature. These atmospheric profiles are interpolated to the heights of the 100 layers in the RTM, using a piece-wise linear distribution for temperature and piece-wise exponential distributions for pressure and water vapor. The CICS retrievals were performed for the C3VP site in the winter season for AMSU-B and MHS.

Nagoya University (Nagoya): Land surface emissivity is computed through (2) [11]. Atmospheric profiles of temperature, humidity, and cloud water (required to compute optical thickness τ) are taken from the Japan Meteorological Agency Reanalysis (JRA)-25 data set. This equation is applied to TRMM TMI TB together with, unlike other existing algorithms, the TRMM Precipitation Radar (PR) for rain-screening purposes. The surface emissivity is first obtained for rain-free

scenes as identified by the absence of rain via PR and then spatially matched up with TMI measurements on a $0.2 \times 0.2°$ global grid. Rain-free surface emissivity is next interpolated across the raining scenes in the close vicinity by applying the Gaussian-weighted average

$$\varepsilon_{\mathrm{i}} = \frac{\sum \varepsilon_{\mathrm{j}} \exp\left(\frac{-d_{ij}^2}{\sigma^2}\right)}{\sum \exp\left(\frac{-d_{ij}^2}{\sigma^2}\right)} \qquad (3)$$

where d_{ij} is the distance between the gridded TMI observation i and TMI observation j (e.g., adjacent observations), and σ is the correlation length, defined here as 0.1 deg, and the summations are performed over j. Raining areas unaccompanied by any rain-free pixels within $d_{ij} = 0.4$ are excluded from the present analysis. The Nagoya emissivity estimates contain three different sets of values: 1) $1 \times 1°$ rain-free emissivity, 2) all-area emissivity averaged over $1 \times 1°$, and 3) all-area emissivity at the original spatial resolution ($0.2 \times 0.2°$). For this intercomparison, the third set of emissivity estimates is used.

B. Emissivity Model Estimate

The most precise method to derive land surface emissivity is through direct computation and estimation through LSMs and emissivity models developed from direct measurements. A wealth of information is available at frequencies at or below 37 GHz; however, emissivity computation and models (based on direct measurements) are less known for frequencies above 85 GHz, many of which are extremely useful for cold season precipitation estimation over land.

NASA/GSFC-Land Surface Model Forward Calculation (LSM): Emissivity is simulated with a Land Information System-Community RTM (LIS-CRTM) developed at NASA Goddard Space Flight Center (GSFC) and at the Joint Center for Satellite Data Assimilation (JCSDA) [27]. Although LIS has several LSMs available, for this study, LIS is run with the community Noah LSM (Vers. 2.7.1) [28]. Because the LSM requires atmospheric boundary conditions or forcings to produce dynamic land surface states, GDAS and the NOAA Climate Prediction Center Merged Analysis of Precipitation 5-day precipitation totals are used. LIS/Noah is configured on a $1/4°$ grid surrounding each target site, using the University of Maryland land cover classification and the Food and Agriculture Organization soils data to provide vegetation and soil types. The outputs of LIS/Noah, including dynamic soil moisture contents, soil temperatures, land surface temperatures, and snow depths, are then used as hourly inputs to CRTM's land emissivity model for the entire study period. CRTM computes land surface emissivity for various surface types using a two-stream radiative approximation [29]. Treatment of roughness and scattering parameters is handled through various physical models such as geometric optics and dense media theory. The model takes satellite zenith angle, frequency, soil moisture content, vegetation fraction, soil temperature, land surface temperature, and snow depth as inputs and computes surface emissivity at vertical (V) and horizontal (H) polarizations. For snow conditions, an empirical approach is taken to compute the emissivity via a combi-

nation of satellite window channel observations and emissivity databases collected from ground-based microwave instruments [30]. A key component in the model is the relationship that maps the window channel observations to the snow type [30]. The mapping algorithms have been developed for AMSU-A, AMSU-B, AMSR-E, and SSM/I. Once a spectrum is identified, it is then adjusted for the requested zenith angle by using the land emissivity model [29]. For other sensors, or when the window channel measurements are not available, the snow surface emissivity (V and H polarizations) is set to a value of 0.92.

C. Physical Retrievals

Physical models which utilize multifrequency PMW observations, sometime in conjunction with ancillary data, can be utilized to retrieve several geophysical parameters simultaneously. The advantage of such techniques is that there is a physical constraint placed upon the retrievals, where the various parameters being retrieved must be consistent with one another. The two techniques described below can retrieve both surface emissivity and land surface temperature.

NOAA/Microwave Integrated Retrieval System (MIRS): Retrievals of emissivity spectra from multiple TB are performed consistently over land, ocean, sea-ice, snow, and coastal areas, using 1-D variational approach (1DVAR) in the MIRS [31]. The emissivity spectrum is contained in the retrieval state vector which also includes temperature and moisture profiles as well as skin temperature and cloud/hydrometeors parameters. The CRTM is used as the forward operator in MIRS, which makes it possible to perform the retrieval in all-weather conditions. Both radiances and Jacobians with respect to all geophysical parameters including emissivity are provided by CRTM. The problem is ill-constrained, but this is alleviated by performing the retrieval in a reduced space, selecting only a limited number of degrees of freedom via an eigenvector analysis. The algorithm is applied and the full emissivity spectrum retrieved for the NOAA-18, 19 and Metop-A AMSU-A and MHS sensors, the DMSP F-16 SSMIS sensor, and the AMSR-E sensor. The 1DVAR algorithm relies on covariance matrices. Those related to the emissivity are computed offline using an ocean emissivity model for the case of ocean and analytically determined emissivities for the nonocean cases.

Physical Emissivity Retrieval (NRL): The microwave surface emissivity is calculated using WindSat RTM and retrieved land surface parameters of soil moisture, vegetation water content, and land surface temperature. The land surface retrievals of these parameters are based on a multichannel maximum-likelihood algorithm using 10 to 37 GHz PMW channels. The algorithm outputs were validated against multiscale data including soil moisture climatology, ground *in situ* network data, precipitation patterns, and vegetation data from AVHRR sensors [4]. The surface parameters considered by the algorithm include soil moisture, vegetation water content, land surface temperature, surface types, precipitation, and snow cover.

For a land surface with a layer of vegetation canopy, the land surface emission is approximated using the $\tau - \omega$ model [32]

$$\varepsilon_{\mathrm{p}} = \varepsilon_{\mathrm{sp}} \exp(-\tau_{\mathrm{c}}) + (1 - \omega_{\mathrm{p}})(1 - \exp(-\tau_{\mathrm{c}}))$$
$$\times (1 + r_{\mathrm{sp}} \exp(-\tau_{\mathrm{c}})) \quad (4)$$

where $\varepsilon_{\mathrm{sp}}$ and $r_{\mathrm{sp}} = 1 - \varepsilon_{\mathrm{sp}}$ are the desired soil emissivity and reflectivity at polarization, p, respectively; ω_p is the vegetation single scattering albedo; τ_c is the slant vegetation optical depth. The first term is soil emission attenuated by vegetation. The second term represents emission contribution from vegetation. TB is then estimated via (2).

The soil emissivity ($\varepsilon_{\mathrm{sp}}$) and reflectivity ($r_{sp}$) are influenced mainly by soil moisture (m_v), and, to a lesser degree, soil texture and surface roughness. Soil moisture increases the dielectric constant of soil-water mixture and thus decreases the soil emissivity; the surface roughness increases scattering and surface area, resulting in an increasing soil emissivity. Within the WindSat retrieval, the surface reflectivity is parameterized empirically [33]

$$r_{sp} = [(1 - Q)r_{op} + Qr_{oq}]\exp(-h) \tag{5}$$

where p and q are orthogonal (vertical and horizontal) polarizations. r_{op} is the reflectivity of the smooth surface and can be computed using the Fresnel equation and a dielectric mixing model, and h and Q are empirical rough surface parameters that are related to the emissivity enhancement and polarization mixing effects due to surface roughness [34]. This simple parameterization is sufficient for modeling soil surface emission for most applications [35].

IV. RESULTS

There are several aspects of the emissivity calculations that need to be examined. In addition to their means and variances, sensitivity to sky conditions (e.g., clouds and precipitation) is of considerable importance to our application. In particular, perhaps the single most important question is the sensitivity of the surface changes during active precipitation: the lower frequency channels should be more transparent to the atmospheric conditions and the most sensitive to ground surface wetting. The complexity is compounded by the typical larger field of view (FOV) sizes on the conical sensors with lower frequency. Additionally, consistency within polarization and across the full frequency spectrum is also important, as specific surfaces will respond in physically consistent ways.

As discussed, some approaches estimate emissivity from a known surface temperature given an observed TB, as in (2). However, not all approaches listed in Table I use the same surface temperature, and it was found that they vary by as much as 3% on the monthly mean time scale and even greater for any instantaneous retrieval. This is shown in Fig. 2, where the monthly mean emissivity under clear sky conditions for the SGP site at 37 GHz vertical polarization is presented for several of the techniques, along with the surface temperature and the product of the two. (This channel will be critical for use in the GPM-era physical retrieval algorithms, as it is affected by cloud and rain drops). As can be seen in the top most panel, it is difficult to discern any coherence in the emissivity data sets over time, with the peak differences among the techniques being on the order of 5%; it should be noted that these differences were smaller at the lowest frequencies and greatest at the higher frequencies. Surprisingly, there is considerable spread in the surface temperature data (middle panel of Fig. 2), with
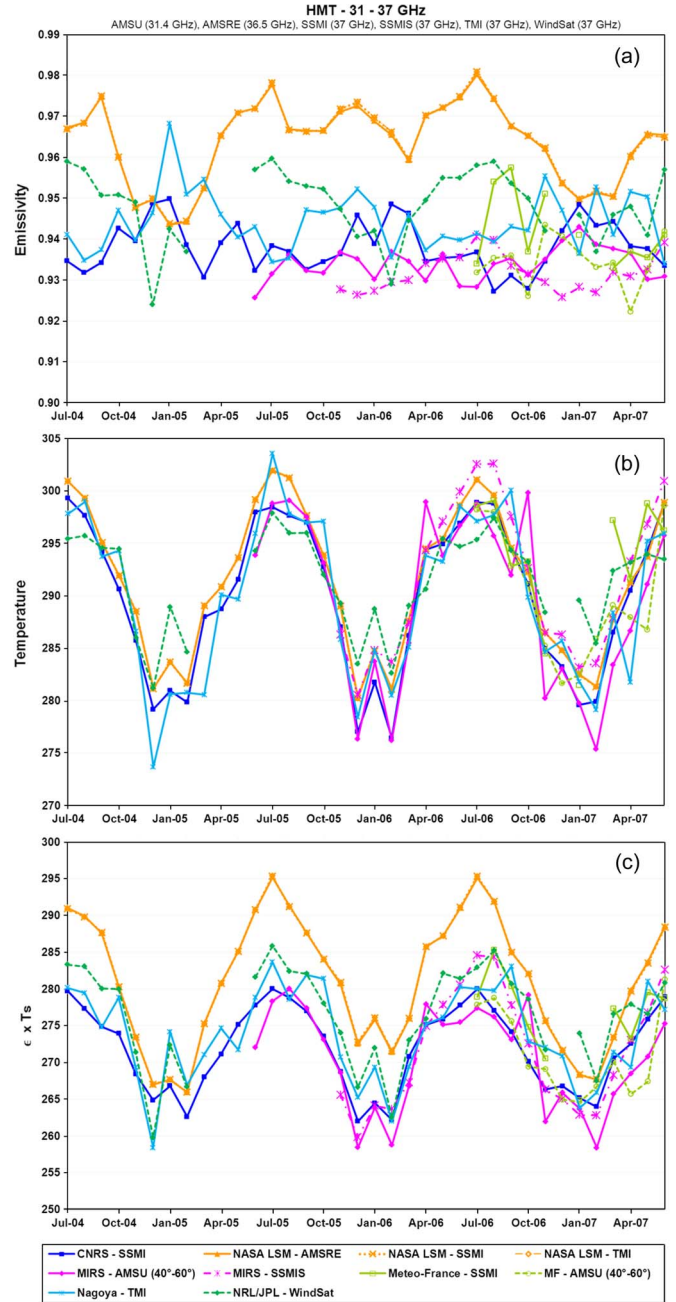

Fig. 2. (a) Monthly mean emissivity at 31 and 37 GHz (for vertical polarization for imagers and mixed polarization for AMSU/MHS), (b) surface temperature and (c) the product of the two for SGP for the time period July 2004 to June 2007. The means include all available data under clear sky conditions.

differences on the order of 2%, or 5 deg K. However, this is comparable to results found by others retrieving surface or skin temperature from sensors such as AMSR-E [36], [37]. There is somewhat of a tendency for those algorithms with the (lower) higher emissivity values to have (higher) lower surface temperatures; this most likely results in how the various retrieval types decompose the satellite TB through (2) [and (2a)]. Finally, when examining the product of the two data sets (bottom panel of Fig. 2), there appears to be a more coherent set of curves over the three year time series and perhaps a better clustering within the classes of retrievals are previously described. Additionally, the maximum differences are on the order of 3%.
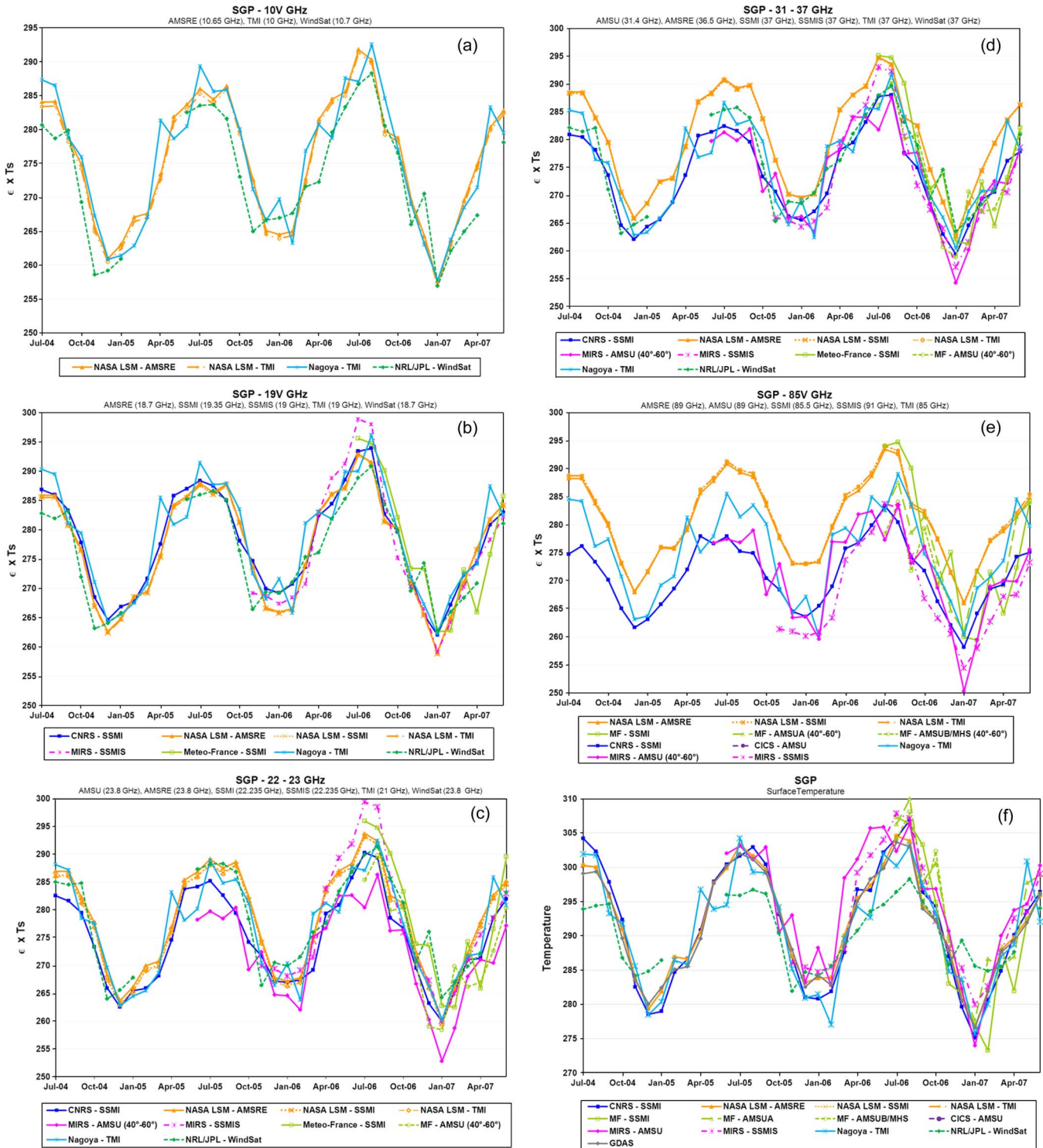
Fig. 3. Monthly mean emissivity (for vertical polarization for imagers and mixed polarization for AMSU/MHS) times surface temperature for SGP site for various frequencies and algorithms for the time period July 2004 to June 2007. The means include all available data under clear sky conditions. (a) 10 GHz, (b) 19 GHz, (c) 22 and 23 GHz, (d) 31 and 37 GHz, (e) 85, 89, and 91 GHz, and (f) surface temperature.

As presented in the previous section, the main driver for the satellite measurement comes from the product of the surface temperature and emissivity, and it is that parameter that needs to be accurately estimated for the advancement of the land surface precipitation retrieval algorithms. Therefore, for the purposes of this intercomparison study, we evaluate the different techniques by a metric defined as the product of the retrieved emissivities

and the surface temperature used in the retrievals, in an attempt to "normalize" the data and examine true variability among the various methods and classes of emissivity retrieval. Most of the results presented are for vertical polarization for the imager sensors, although both polarizations were evaluated, whereas the sounders have mixed polarization and are treated slightly differently (as discussed in next section).

The data for the various algorithms, targets, and seasons were analyzed in a number of ways. In this section, an overall seasonal summary is presented for each of the three target areas. Next, the spectral signature of the retrieved emissivities is examined and compared to expected values based on previous studies done over specific surface types. Lastly, the impact of weather conditions on the retrievals is examined. Additionally, throughout much of the paper, similar channels were grouped within the plots (e.g., 31 GHz from AMSU with 37 GHz from the other sensors, etc.) since the emissivity response from surface changes is expected to be similar.

A. Seasonal Summary

Initially, the monthly mean emissivity for all algorithms under clear sky conditions was compared. Here, we focus on the vertical polarizations for the imager sensors whereas the AMSU/MHS data are restricted to view angles between 40 and $60°$ to give comparable results to the conically scanning imagers that typically view the earth with a zenith angle near $50°$. Note that AMSU/MHS skews its polarization basis across the scan swath with it being vertical at a view angle of $0°$; however, for many surfaces, the emissivity varies greater with view angle, thus a decision was made to compare the data in this manner, but it is recognized that it is not necessarily a precise comparison of the data from the different types of sensors (i.e., fixed view angle conical versus cross-track scanners). Each emissivity estimate was matched up with the following closest 3-h data products of ISCCP and CMORPH. Clear sky condition was flagged when the presence of clouds in ISCCP cloud mask was less than 60%, near the neighboring target center, and in the one-degree area, and CMORPH rain product indicates no rain. Then, the mean value was calculated from those estimates that were flagged as clear sky. It was found that these thresholds produced the most stable results across all of the different algorithms. These are summarized first by each of the targets, and then some preliminary conclusions are presented.

SGP: The SGP site (35N 97W) located in central Oklahoma is an agricultural region of pastures and wheat fields that experiences seasonality much like HMT-SE; however, it is a more arid climate due to its distance from any large body of water. In terms of sensible weather, it experiences more extremes that at HMT-SE; greater seasonal and diurnal temperature changes, prolonged periods of dry weather, but can also experience strong convective rains in the springtime and can be subject to heavy snowfall in the winter. It is a very homogeneous region of mostly flat terrain that is mostly used for agriculture [38].

Fig. 3 shows the monthly mean $\varepsilon * T_s$ for all available frequencies (V polarization), sensors, and data sets. In general, all of the estimates show the same general trend in seasonal and interannual variability, apparently due to surface characteristic changes like vegetation cover (spring to summer to fall) and snow cover (winter); the degree of the variations from year to year would be reflective of interannual differences in vegetation and snow cover; however, the largest variations are the annual cycle. Examining the data more closely, one can see that the dispersion among the techniques increases with increasing frequency, not unexpected since the complexity of
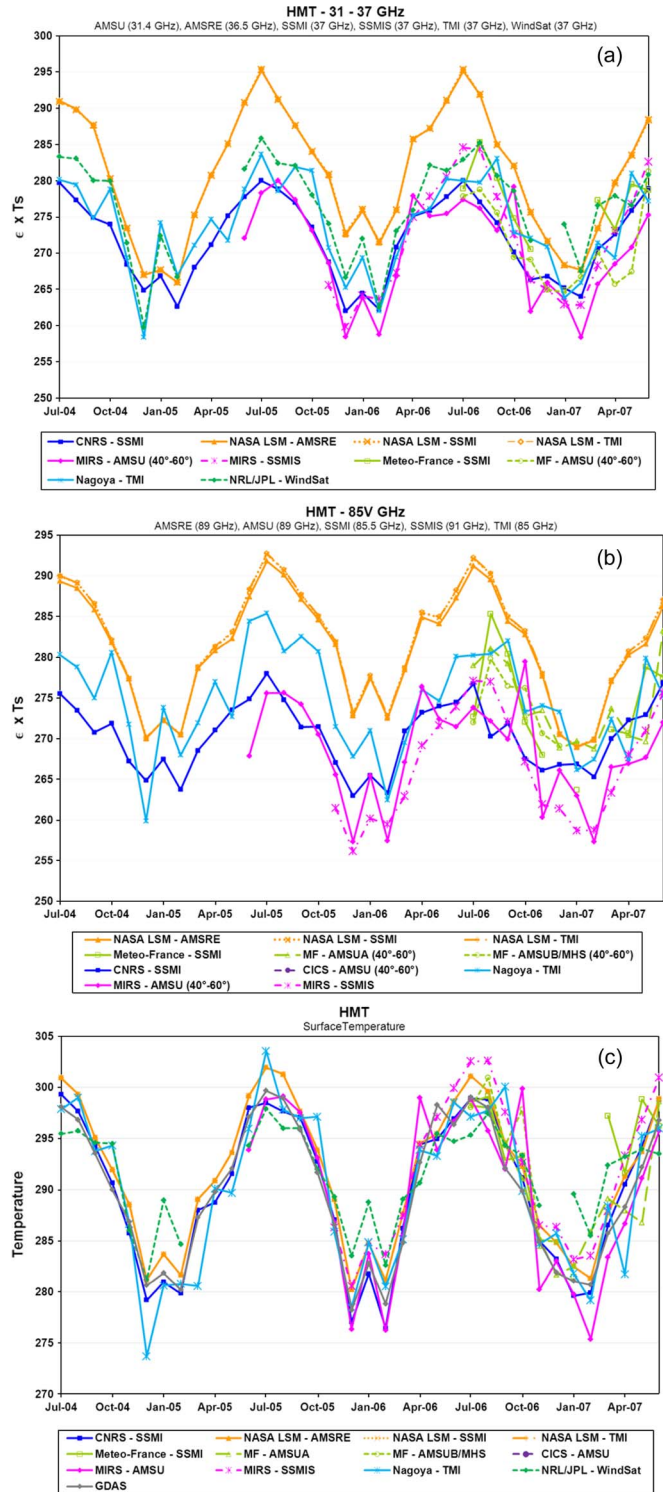

Fig. 4. As is Fig. 3, but for the HMT-SE site and for (a) 31 and 37 GHz, (b) 85, 89, and 91 GHz and (c) surface temperature.

surface emissivity as well as atmospheric affects are larger at the higher frequencies.

Examining the differences among the different data sets, it is apparent that the LSM estimates tend to be higher than the others, particularly evident at 37 and 85 GHz, where perhaps the ISCCP cloud screen has missed cloudy scenes (emission from nonprecipitating water droplets greatly affects the microwave emission) and are impacting the inversion type
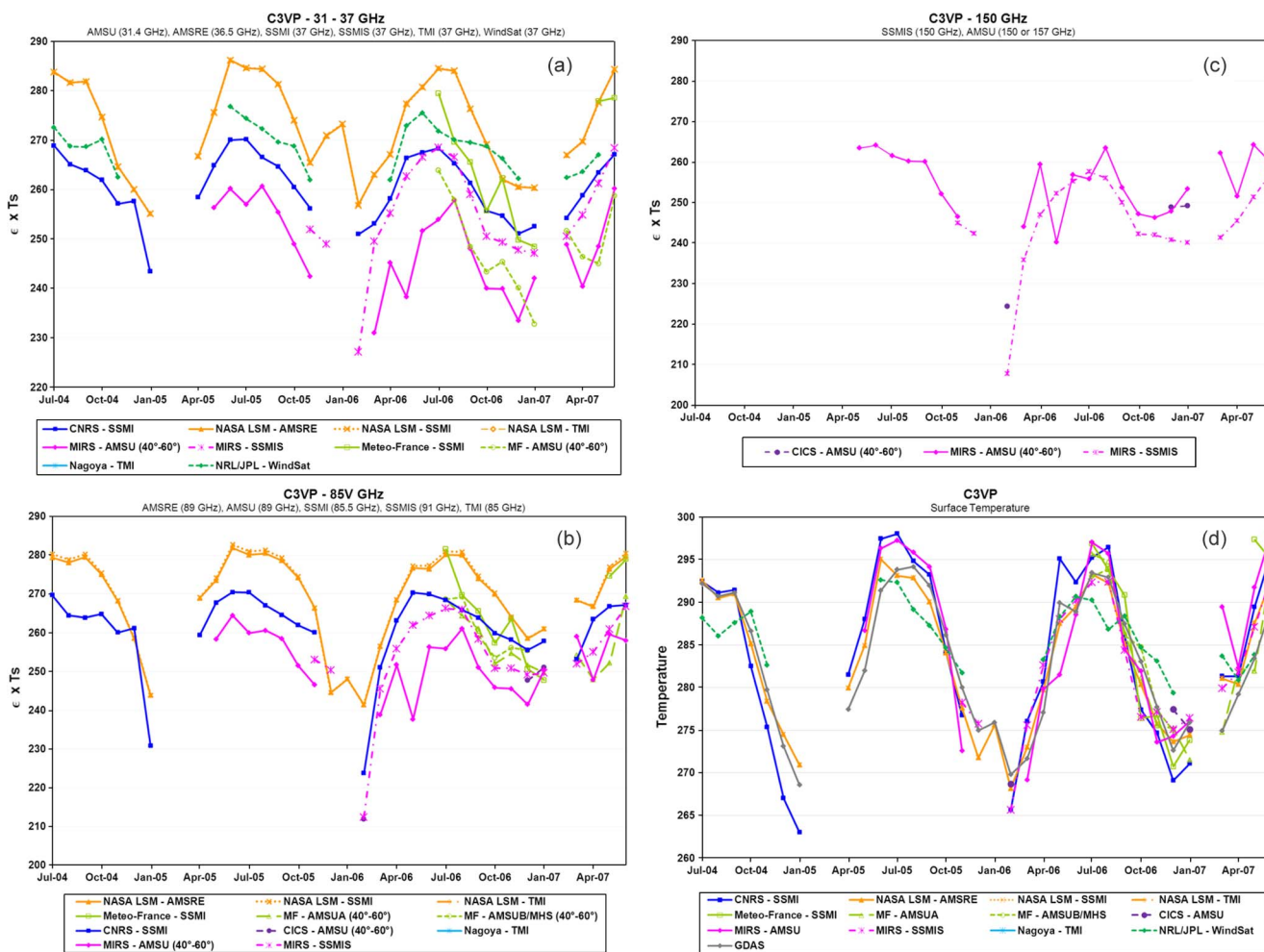
Fig. 5.   As in Fig. 4, but for the C3VP site and includes (c) 150/157 GHz and (d) surface temperature.

emissivity retrievals. On average, the differences noted at these frequencies can be as large as 10 K on the monthly mean, which is well beyond the signal due to liquid water or ice crystal from light precipitating conditions [39].

The Ts are shown in panel (f); note that there is considerable spread in the data. Some differences are due to the type of the retrieval; the physical schemes (e.g., MIRS and NRL) show some differences from the inversion schemes whereas the LSM is not too different from GDAS, which was the baseline in this study. Other inconsistencies may be attributed to different "sampling" among the various techniques, i.e., not all of them provided same set of instantaneous retrievals over the month due to differing conditions within their own retrieval. This theme is essentially the same across all three targets.

HMT: The HMT-SE site, henceforth referred to as HMT, experiences seasonal changes typical of a midlatitude continental site. Centered at (36N 81W) on the Tar and Neuse River Basins of Central North Carolina, it is in an area of rolling hills of between 100 m and 500 m in an area which is highly forested and experiences seasonal vegetation changes. It can experience a wide range of precipitation ranging from prolonged stratiform rains, heavy convective rains (and periodically, flooding rains from land falling tropical systems), and occasional snowfall [40].

Fig. 4 shows similar plots as in Fig. 3, but here we focus just on 37 and 85 GHz; two channels critical for precipitation retrieval. Although not shown, the results at 10, 19, and 22 GHz at HMT were very similar to what was found at SGP; however, LSM tended to be higher during the warm seasons when compared with NRL and Nagoya (both of which agreed very closely at 10 GHz) and the other estimates at 19 GHz. MIRS tended to be the lowest as was the case at SGP. Similarly, that basic trend is evident at 31/37 and 85/89/91 GHz, and the dispersion among the different data set increases with increasing frequency. The effect of the atmosphere is a possible cause for the persistent 5–10 K difference between LSM and the satellite-based techniques. At the highest frequency, the two MIRS data sets from AMSU/MHS and SSMIS are rather consistent, a testimony to the physically consistent approach used within MIRS.

C3VP: The C3VP site (44N 80W) is perhaps the most complex of the three sites in terms of geography and weather. It is located in southeastern Ontario just to the northwest side of Lake Ontario and a mixture of land and water, as well as forests, woodlands, and grasslands [41]. There is a pronounced winter season with extended snow cover; this site was selected because of GPM's extension into winter season precipitation and the challenges that it faces with characterizing the snowpack and its impact at microwave frequencies [42], [43].
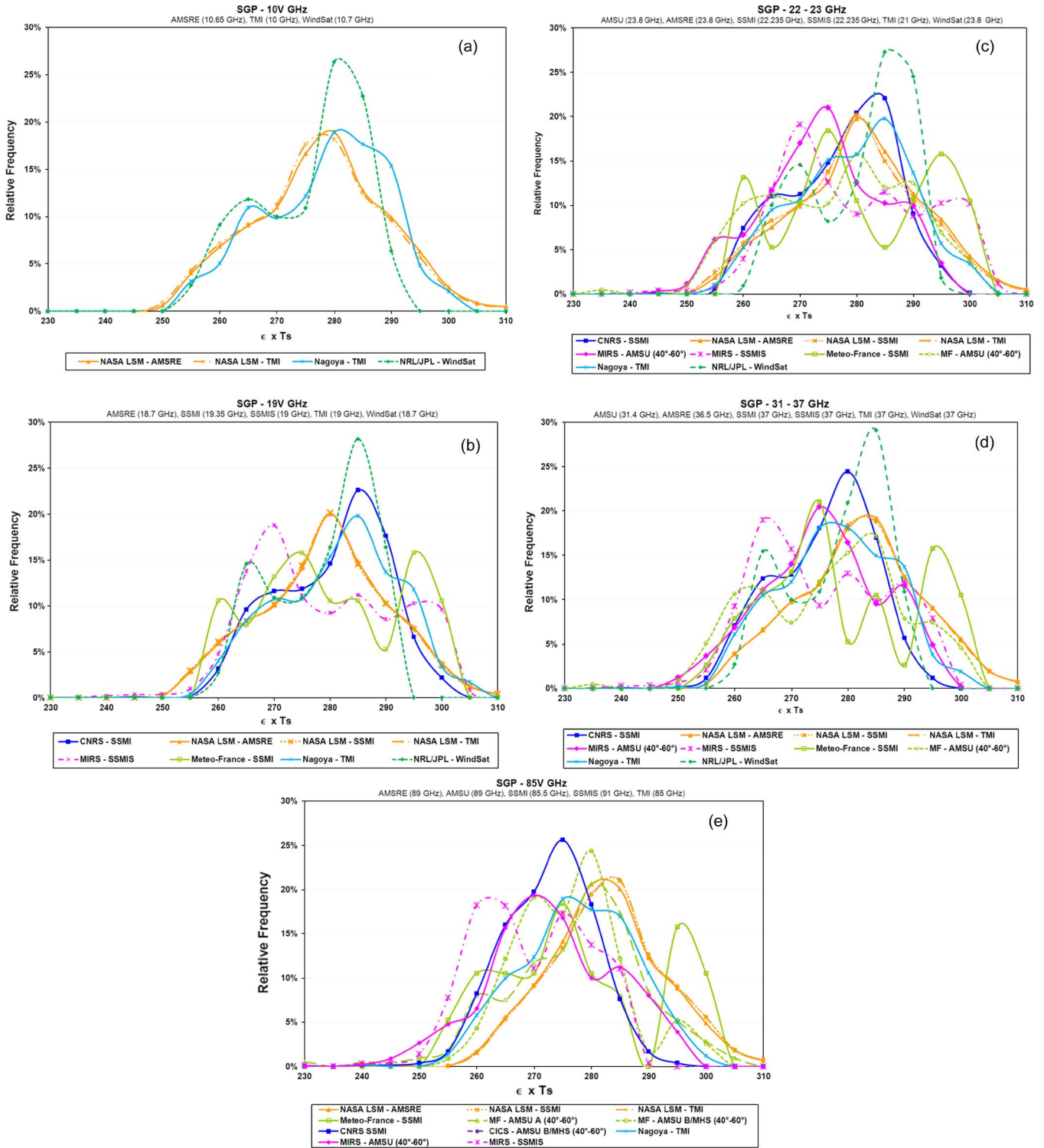
Fig. 6. Probability distribution functions (PDF) for SGP for all frequencies (vertical polarization for imagers, mixed for AMSU/MHS), algorithms and combined for all time periods for clear sky. (a) 10 GHz, (b) 19 GHz, (c) 22 and 23 GHz, (d) 31 and 37 GHz, and (e) 85, 89, and 91 GHz.

Fig. 5 shows similar information as Fig. 4, but for the C3VP location. Here, we also include measurements from 150 GHz since this channel is critical in detecting falling snow [44]. Note that this site is out of TMI coverage, so fewer estimates are available for the comparison; however, the NOAA-CICS data are available for this site. Unlike the previous two sites, the dispersion at C3VP is greater even at the lowest frequencies between 10 and 23 GHz. Some things are consistent; LSM has the greatest values and MIRS the lowest. In general, a larger dynamic range is seen during the annual cycle due to the colder nature of this site [i.e., compare Fig. 5(d) with Figs. 4(c) and 3(f)] and persistent snow cover that exists during the winter season. Additionally, differences in Ts are noted, in particular, with the physical retrieval techniques, which are apparently a large reason for the lower/higher values with MIRS/LSM.

Referring to the higher frequencies (Fig. 5), a wide range of values are seen across all of the estimates, although they generally track the seasonal to interannual variability in a similar manner. Note that there are some months without any estimates due to a lack of clear sky data at the site, which can be dominated by low clouds in the winter months. During the cold seasons, some estimates show a wider dynamic range (e.g., MIRS and MF) at 37 GHz, although this is not necessarily any worse at 85 GHz. A possible explanation is the effect of snow grain size impacting the estimates at 37 GHz more than at 85 GHz [13], [14].

B. Probability Distribution Functions (PDF)

The monthly means provide general idea of how the estimates compare in the broad sense and also capture seasonal to interannual variability. However, a more important aspect that is vital for the precipitation community is how much variability exists on an instantaneous scale for the different techniques and locations. This is examined more closely through the use of clear sky PDF's. In the sections that follow, clear sky data are used, and all of the instantaneous retrievals for each technique for all days, months, and years are presented in the PDFs.

SGP: Fig. 6 presents PDFs of across all frequencies (vertical polarization) and instruments for $\varepsilon * T_s$ for clear sky data. As was the case for the monthly mean data, this product tends to normalize the data (i.e., if the raw values of emissivity were shown, there would be pronounced shifts of the peak PDF values).

At 10 GHz, all four data sets presented have a tendency to show a bimodal type of distribution; with peaks are 280 K and around 265 K. This is most pronounced in the NRL/JPL and Nagoya estimates. The NASA/LSM shows the broadest distribution, perhaps again due to the lack of atmospheric contamination as well as temperatures from the LSM energy balance. The PDFs at 19 GHz are more complicated to interpret; however, there again is a tendency for bimodal distributions, but with the peaks not as precisely defined as was the case at 10 GHz. The PDFs at the water vapor channels near 23 GHz and also at 31/37 GHz are a little more self-consistent than at 19 GHz. At 85/89 GHz, there is less evidence of a bimodal structure, and the satellite-based techniques tend to show a peak at lower values than those from NASA/LSM. The systematic differences between the satellite-based techniques and the NASA/LSM forward technique at higher frequencies relate to assumptions in the CRTM forward model at high frequencies as well as possible cloud contamination in the satellite-based techniques. The bimodal character in the data might be attributed to diurnal variations; however, it is also evident in the TMI data, which should be sampled equally across the day. However, one might expect that this could be an influence with the polar orbiting satellites like Aqua, DMSP, and WindSat.

HMT-SE: Fig. 7 presents the PDFs for the HMT-SE site; here, just 23, 31/37, and 85/89 GHz are examined. There are similarities and differences with the 23 GHz data at HMT when compared to SGP; the relative peak values of $\varepsilon * T_s$ among the various algorithms are somewhat consistent; however, there tends to be more disparity among the different data. Perhaps,
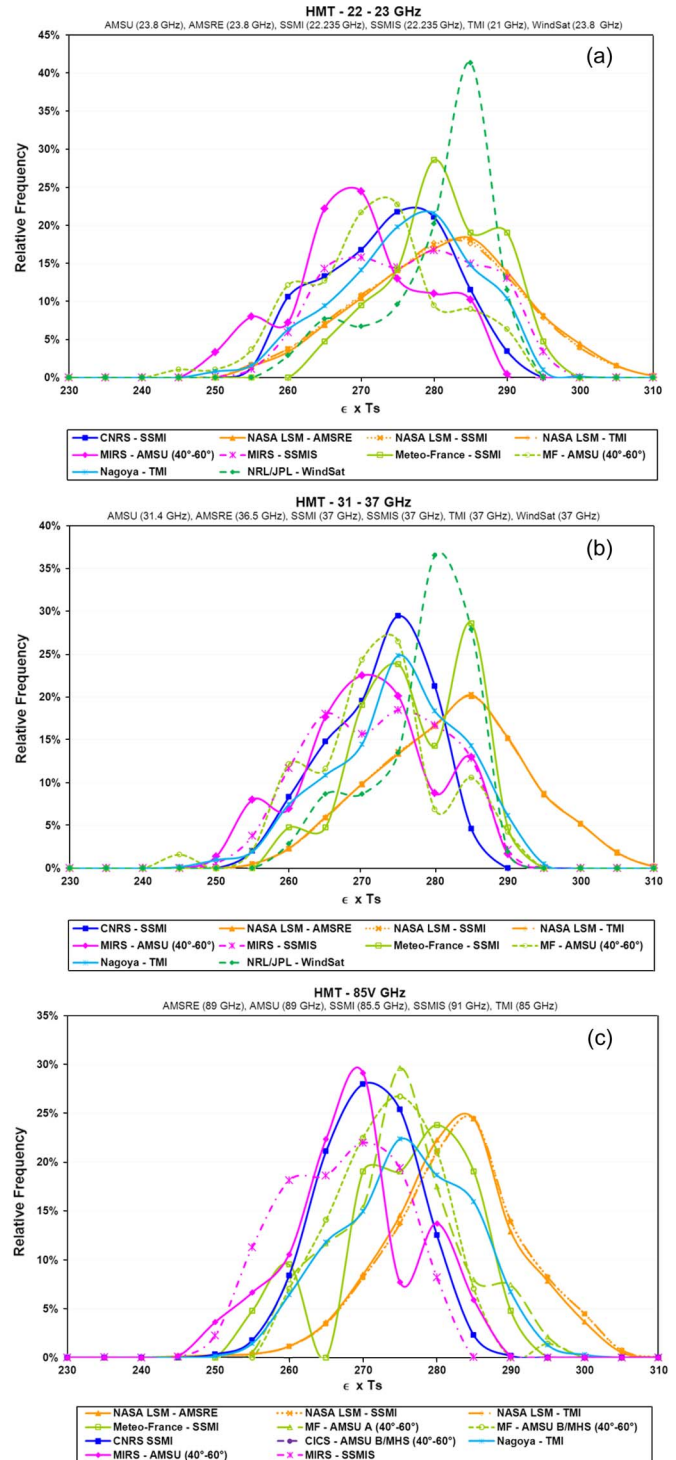

Fig. 7. As in Fig. 6, but for HMT-SE site and for (a) 22 and 23 GHz, (b) 31 and 37 GHz, and (c) 85, 89, and 91 GHz.

the moisture environment at HMT versus SGP is a possible explanation. In addition, the MF and MIRS data appear tend to be somewhat different as compared to the other estimates; perhaps, a lack of convergence within those schemes under certain meteorological situations is a possible explanation. Better agreement is evident at 31/37 GHz, and also there is consistency to what was found at SGP. Finally, at 85/89 GHz, there is a clear separation in the peak values between LSM and the satellite
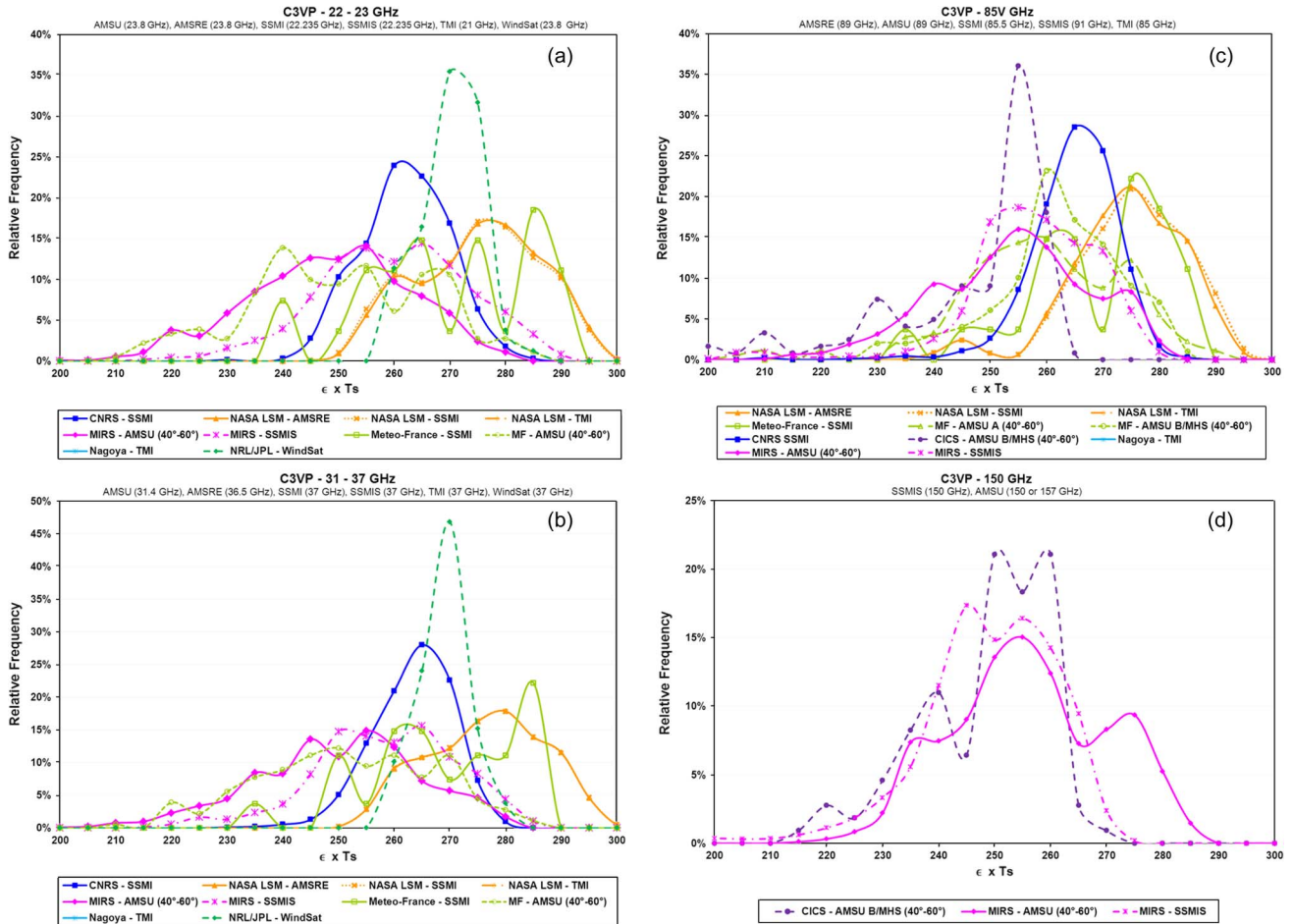
Fig. 8. As in Fig. 7, but for C3VP site and for (a) 22 and 23 GHz, (b) 31 and 37 GHz, (c) 85, 89, and 91 GHz, and (d) 150 and 157 GHz.

data. This is similar to what was seen at SGP; however, the disparity at HMT is greater. Again, atmospheric moisture contamination in the satellite-based estimates, coupled with issue in the CRTM emission model as well as LSM temperatures might be a plausible explanation.

C3VP: A similar analysis was performed for C3VP, and the results are presented in Fig. 8. Compared with the previous two locations, the range of data values at C3VP is much larger, in particular, at the low end. This is due to the greater seasonal variations in surface temperature, atmospheric moisture, and periods of persistent snow cover. Hence, the results indicate the largest spread among the various data. This demonstrates the difficulties in doing precipitation retrievals in cold seasons. Aside from LSM showing a peak value at a higher value of $\varepsilon * T_s$ compared with the satellite derived values, further conclusions are difficult to come by for 23, 31, and 85 GHz. In the case of the LSM-derived estimates, a major issue causing the discrepancies that is not as prominent at the other sites relates to the presence of snow cover at the C3VP site, which in turn causes the emission model in CRTM to adopt higher values than observations. This issue is being addressed in the next CRTM release, with an updated snow emission model.

As previously discussed, the HF channels are attractive for use with cold season precipitation. Although the number of emissivity retrievals at 150 GHz is limited in this study, Fig. 8(d) shows the PDFs for the MIRS and CICS estimates.

Surprisingly, there is relatively good agreement among the data, yielding promise in the use of such data for the retrieval of falling snow.

C. Spectral Signatures

Other important aspects of the emissivity estimates to examine are the spectral response, differences between vertical (V) and horizontal (H) polarizations, and their seasonal changes. All of these properties are critical for algorithm development for precipitation retrievals since multifrequency techniques are typically employed [3], [31], [39]. It has been shown in several studies that the relationship among all of these parameters is fairly well known for various surface features. In the case of the three target areas, the predominant surface types would be vegetation cover, potential snow cover, and varying soil moisture.

Because the C3VP site experiences the most dramatic seasonal changes of the three that are being examined in this study, the comparison of the spectral signatures will focus on this location; however, the results from the other sites are fairly consistent to those found at C3VP. Shown in Fig. 9 are the mean emissivities as a function of frequency and season for both V and H polarizations for each technique. The data plotted are for all three years (where available) and are for clear sky data only. It should be noted that this information is only provided for the
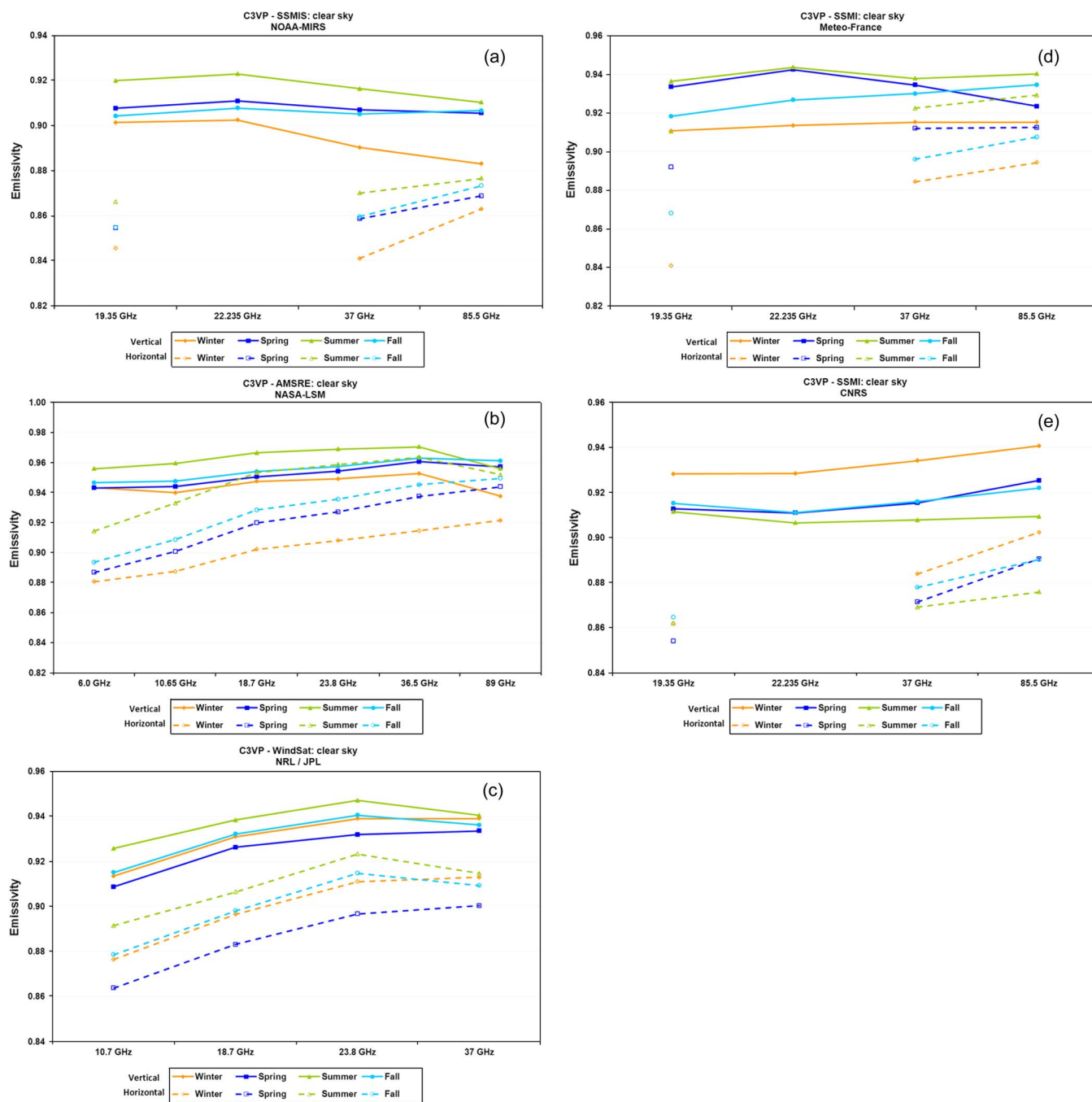
Fig. 9. Seasonally averaged emissivity spectrum for V (solid) and H (dashed) polarization for the different data sets at the C3VP site: (a) MIRS, (b) LSM, (c) NRL, (d) MF, and (e) CNRS.

conically scanning sensors and techniques. Also, since Nagoya only generates estimates for TMI, no data exist for the C3VP site since it is too far north.

Under vegetated conditions, a flat or slight increase in emissivity with frequency is expected whereas when vegetation is low, then a more dramatic increase in emissivity with frequency would be expected [1], [4], [12], [14]. When snow cover is present, a potential decrease in emissivity at or above 37 GHz is anticipated [13]. Additionally, V is greater than H polarizations except for under very dense vegetated conditions where the two would be very close in magnitude. With this in mind, the results presented in Fig. 9 can be interpreted.

First examining the season variability, MIRS shows the widest range between V and H polarizations and the largest decrease in emissivity value between low and high frequencies during summer and more pronouncedly in winter; the other techniques show less of a dynamic range difference between V and H and generally show a flat or slight positive slope in emissivity with frequency. The season of maximum emissivity also varies among the data, with most showing the highest values in the summer (due to maximum vegetation cover) and the lowest in winter, while the transition seasons are in between. CNRS appears to be an outlier, with the highest values in winter and lowest in summer, although this has been traced to surface
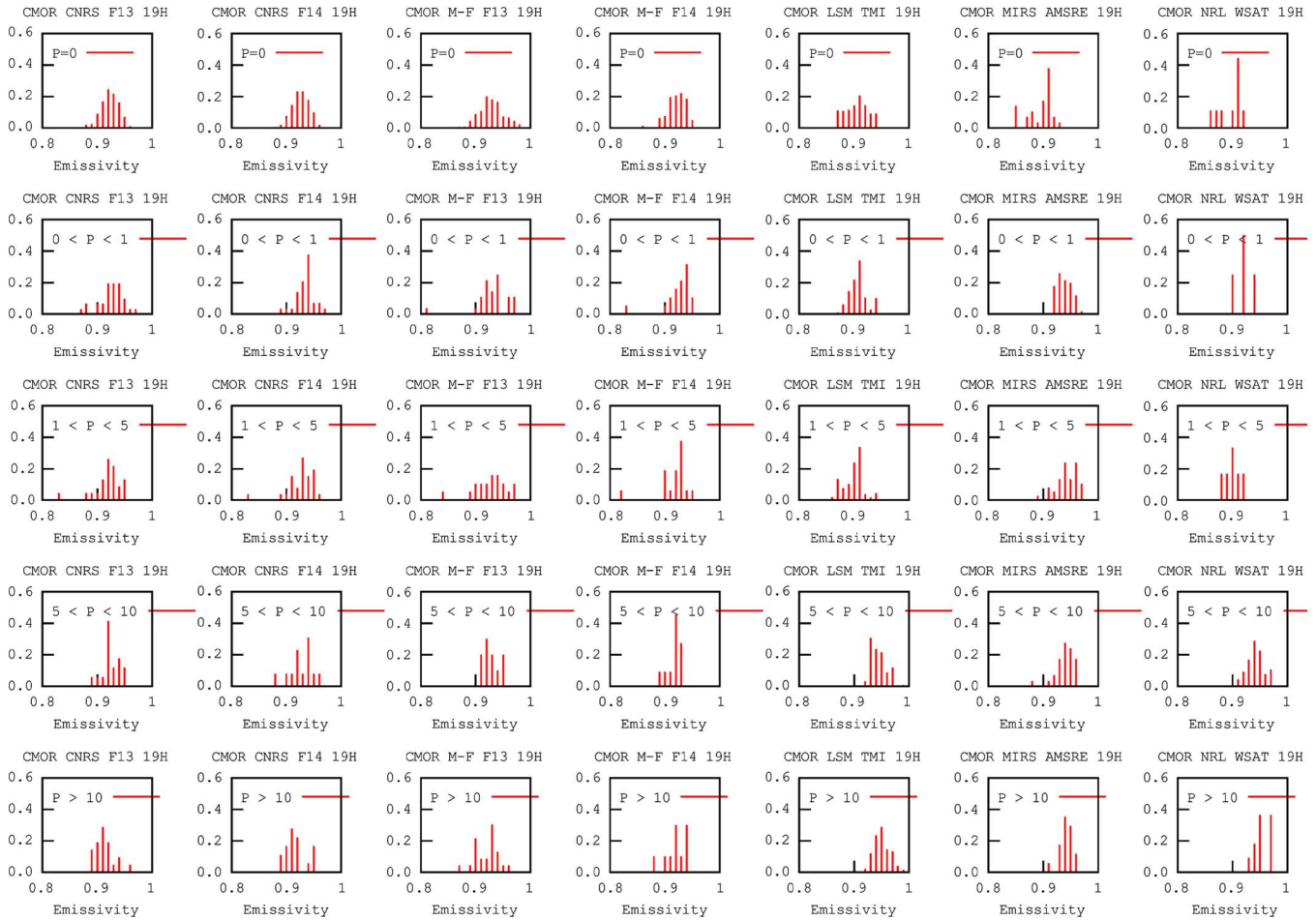
Fig. 10. Histograms of the 19H GHz emissivity, for seven different emissivity products, separated by the amount of previous-time precipitation, for the June 2006–July 2007 period over the SGP site. Each column indicates the emissivity product, and each row refers to the amount of previous one-day precipitation (mm). The seven emissivity products (left to right) are the CNRS SSMI F13, CNRS SSMI F14, Meteo-France SSMI F13, Meteo-France SSMI F14, GSFC LSM TMI, NOAA MIRS AMSR-E, and NRL WindSat. The five precipitation intervals are, top to bottom, $P = 0$, $0 < P < 1$, $1 < P < 5$, $5 < P < 10$, and $P > 10$, where P refers to the previous one-day accumulations in mm.

temperature affects. Many of the techniques show a decrease in emissivity at 85/89 GHz in the winter season which can be attributed to snow cover, so it is encouraging to see this expected feature in the data. Finally, all of the estimates show the expected consistency between V and H polarizations, with the former being greater in every instance across the range of frequencies being evaluated. However, the magnitude of this difference varies widely over frequency and season.

D. Impact of Weather Conditions and Implications for GPM-Era Algorithms

In this section, the impact of precipitation on surface emissivity is presented through the use of multisatellite precipitation products, which can be matched closely in time and location to PMW satellite overpasses and any associated emissivity estimate. The precipitation products examined were CMORPH, 3B42, and the NRL-Blend. The baseline product for each of these data sets is a three-hourly precipitation accumulation, updated every 3 h, produced on a 0.25-degree rectangular grid between ±60° latitude. These products have found a wide use in many applications, including the ongoing precipitation
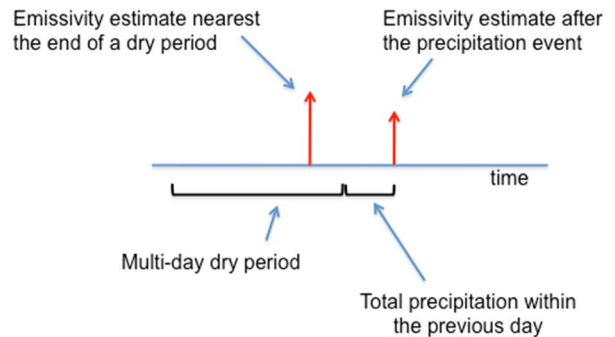

Fig. 11. Illustration of how the data sets were prepared for use in Fig. 4. The total one-day precipitation preceding the emissivity estimate was located, as well as the time duration of the period of no-rain (dry period) just before the one-day precipitation interval. This enables one to find the duration of the dry period prior to the rain, as well as the emissivity estimate closest to the end of the dry period. The percent change between these two emissivity estimates is examined as a function of the dry period and the one-day precipitation.

validation project of the International Precipitation Working Group [45], [46]. These precipitation data sets can be used to locate when and how much precipitation fell in time intervals prior to the PMW satellite overpass covering each of the LSWG regions. Analysis from these precipitation data provides a
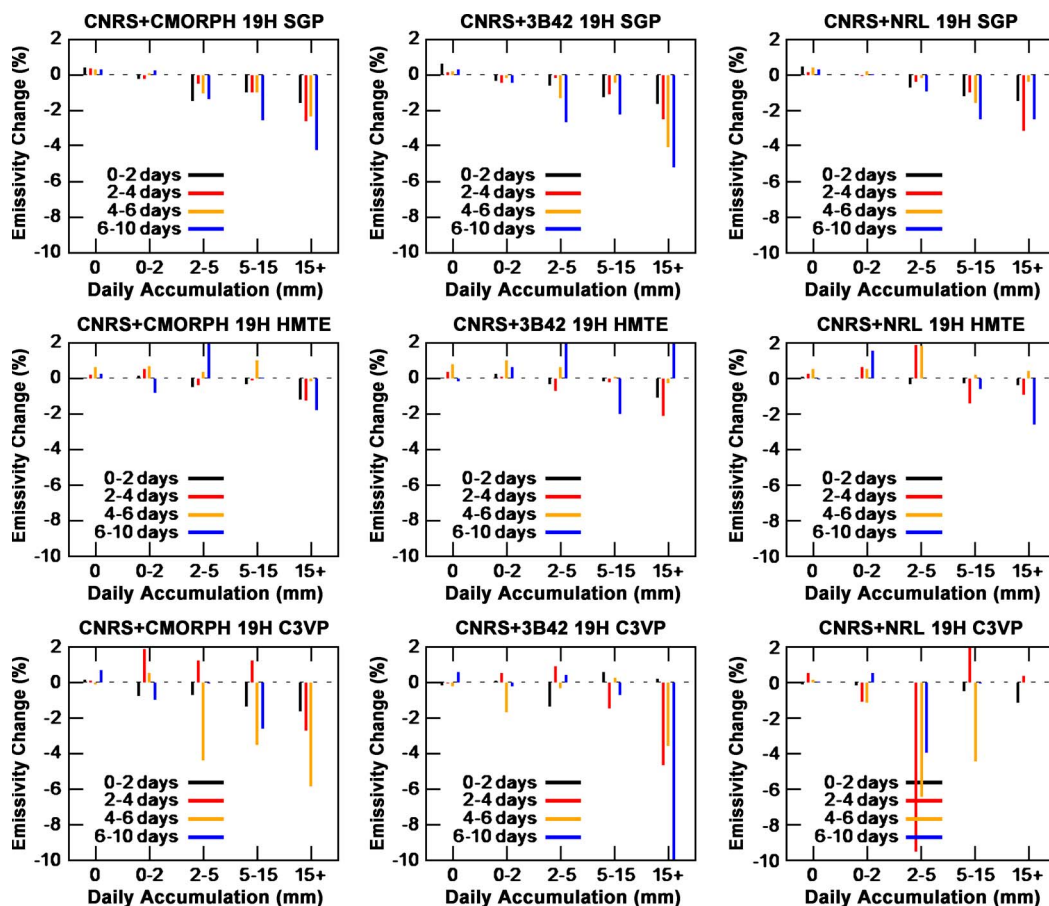
Fig. 12.   Percent change in the 19H emissivity, for different previous one-day precipitation accumulations (*x*-axis in each panel), and duration of different dry (no-rain) intervals prior to the onset of precipitation (colored impulses in each panel). Top row: CNRS SSMI F13+F14 data over SGP site, using the (left) CMORPH, (middle) TRMM 3B42, and (right) NRL-Blend precipitation data set. Middle row: Same as top row, but for the HMT-SE site. Bottom row: Same as top row, but for the C3VP site.

reference for intercomparison of emissivity estimates from rainfall-wetted surfaces.

Fig. 10 presents histograms of the 19H GHz emissivity, for seven LSWG emissivity products, separated by the amount of previous-time precipitation, for the June 2006–July 2007 period over the SGP site. Each column indicates the emissivity product, and each row refers to the amount of previous one-day precipitation (mm) from the CMORPH technique. The seven 19H GHz emissivity products (left to right) are the CNRS SSMI F13, CNRS SSMI F14, MF SSMI F13, MF SSMI F14, GSFC LSM TMI, NOAA MIRS AMSR-E, and NRL WindSat. The five precipitation intervals are, top to bottom, $P = 0$, $0 < P < 1$, $1 < P < 5$, $5 < P < 10$, and $P > 10$, where P refers to the previous one-day accumulations (mm) from CMORPH over a 1-degree box surrounding the SGP region. During this one-year period, the satellite local crossing time difference between DMSP F13 and F14 increased from 30 min to 1 h, yet there is a fairly good comparison between the F13 and F14 emissivity histogram from CNRS and MF. In the absence of any previous one-day precipitation (top row), the histograms are clustered around a value of $\varepsilon = 0.93$; for $P > 10$, they cluster lower, near $\varepsilon = 0.9$. It is more difficult to extract conclusions from LSM, MIRS, and WindSat as the previous one-day precipitation increases (WindSat has a lengthy revisit time owing to its narrow swath and has the least amount of

samples from which to build the histogram). However, such representation does not properly assess the emissivity response to precipitation, since the surface could have been very dry prior to the one-day rain period, or very wet (i.e, rain falling upon an already wet surface). Furthermore, use of a different precipitation product could produce a different outcome.

To examine further, the CNRS SSMI F13 and F14 data were separated into previous time dry periods, so that the one-day rain period occurred after an interval of time where no rain had occurred. To provide more samples, F13 and F14 were combined, and the analysis period extended between June 2004 and July 2007. Fig. 11 shows the analysis concept. In Fig. 12, the percent change in the 19H emissivity is shown in each panel along the *y*-axis, for different previous one-day precipitation accumulations (*x*-axis in each panel). The time duration of different dry (no-rain) intervals prior to the onset of precipitation is denoted by the colored impulses in each panel. The top row represents the SGP region, using (left to right) the CMORPH, TRMM 3B42, and NRL-Blend precipitation data sets. Similarly, the middle and bottom rows indicate the HMT and C3VP regions. This type of analysis provides an indication of the amount of precipitation needed to produce a noticeable change in emissivity relative to the dry period. For the SGP site, there is essentially no response in the 19H emissivity until after at least 2–5 mm day-1 accumulated rainfall, regardless of the

precipitation data set used. For CMORPH and 3B42, up to a 5–6% drop in the 19H emissivity (slightly less for NRL-Blend) is noted for rain accumulations exceeding 15 mm day-1 following a 6–10 day dry period. However, for the HMT site, there is essentially no signature in the emissivity, from any of the satellite-based precipitation data sets. This is consistent with the higher year-round vegetation content in the HMT region, compared to the agriculturally based SGP site. However, for the Canadian C3VP site, no consistent picture emerges as either the duration of the dry period or the daily precipitation increases. Much of this is attributed to the poor performance of these satellite-based precipitation data sets over highly variable background surfaces (inland rivers and lakes which freeze in winter, snow cover) relative to the ≈40-km resolution of the SSMI 19 GHz channels. The GPM Cold Season Precipitation Experiment (GCPEX) (early 2012) near the C3VP site will produce additional opportunities to test these results and assumptions.

V. SUMMARY

While limited to several small areas, this study represents the first intercomparison specifically focused upon quantitative assessment of the several strategies and approaches for estimation of microwave surface emissivity. With better knowledge of the surface, GPM algorithms can better utilize the information contained in surface-sensitive PMW channels and move toward a detection of the liquid associated with rain and the ice associated with frozen precipitation. It was found that because of apparent differences in the treatment of surface temperature by the various techniques, a more valid comparison could be made when examining the product of the emissivity and surface temperature, and it is the product of these two terms that dominates the satellite measurement and offer the greatest uncertainty in terms of actual measurements that can be made by in situ instruments. Additionally, the different methods were shown to reproduce the overall seasonal characteristics of the underlying surface, but significant differences were noticed from day-to-day, the magnitude of which depends upon the surface type. This was not unexpected, since there are limits to how each technique can tune or adapt to a wide range of atmospheric and surface conditions. This study did provide further direction on how to consistently specify *a priori* information describing the radiometrically variable surface emissivity within a precipitation retrieval algorithm. For example, there is a high degree of correlation between the emissivity at each channel, which suggests that there are some underlying physical processes that are influencing all channels. If the two or three most important of these processes can be extracted, then these could be used to make self-consistent changes to emissivities at all channels.

The purpose of this study was to determine similarities and differences between the various methods for estimating emissivity and how this information can be used to move forward in the advancing the current state of precipitation retrieval over land. We conclude that:

- Confidence in emissivity estimates is greatest in vegetated regions and for frequencies at or below 37 GHz.

- Emissivity can be used explicitly in the precipitation retrievals when the precipitation signal exceeds the surface-related uncertainty. For example, a 3% uncertainty at 19 or 37 GHz is roughly 10 K in TB, certainly good enough for liquid water computations in heavy rain, but not good enough for discriminating rain/no-rain and retrievals of lighter precipitation. Nonetheless, precipitation algorithm developers can move forward in this regard.

- It appears that the impact of precipitation upon the emissivities in the light-to-moderate vegetated area (SGP) is most noticeable after moderate-heavy rain events (exceeding 10 mm in the previous day).

- Although many of the input parameters used by the individual techniques were controlled as much as possible, in many cases, large differences were noticed. Since nearly all global emissivities lie within a very small range (a lower bound of roughly 0.2 for 10 GHz H polarization over ocean, to 0.99 over dry bare soils), different external forcings (e.g., surface temperature, atmospheric opacity, cloud/precipitation screening) strongly influence the range of values among these data sets.

- To test the validity of the LSM estimates, one could "place" the atmosphere on top of the LSM emissivities and then compared simulated TB with observed TB [22]. If the TBs agree well, then likely the emissivities are realistic and within an uncertainty suitable for physical precipitation retrieval techniques. Such a test would also provide a means to indirectly verify or nullify the spectral slope differences that were noticed.

- Complex surface types. The emissivity variability characteristics of such surfaces are highly variable and affected by smaller scale features (leaf area index, snow grain size, etc.) that are variable both in time and spatially within the large satellite footprint. Additional input information upon the terrain and land cover within the FOV (e.g, elevation, slope, and its variability) and dynamic surface cover (e.g., MODIS snow cover or equivalent) within the LSM approach would allow the retrievals to better identify such complex scene conditions, which would be passed on to the precipitation algorithms.

In terms of ongoing and future efforts of the PMM LSWG, the group has undertaken several concurrent studies to establish a more complete description of the surface emissivity for the GPM algorithms, including:

- *Self-similar surfaces*. Gridded emissivity databases are not particularly adapted to the geometry of a conical or cross-track scanning radiometer, whose on-earth footprint location and viewing azimuth varies directionally from orbit to orbit. However, from many years of emissivity retrievals, it is possible to identify surfaces that are largely similar to others (e.g., grasslands, snow cover, deserts), i.e., clustering approaches used to categorize the globe into ten classes based on emissivity [17]). Further clustering will expand upon this approach with clustering technique based both on emissivity and emissivity co-variances.

- *EOF analysis*. There is a high degree of correlation between the emissivity at each channel. This information

can be exploited so that self-consistent changes can be made to the full emissivity spectrum, rather than channel by channel. Empirical orthogonal function (EOF) analyses can be used to describe the emissivity by only a few parameters, but the spectral signatures of the EOFs are likely to be dependent upon surface type.

- *Dynamic emissivity databases.* As shown in this paper, the surface emissivity can change very rapidly with the onset of precipitation. A dynamic database that adapts itself using precipitation information from the previous revisit time could be used to better characterize the "wet surface" emissivity, and how variable these are from the emissivities that were extracted from noncloudy scenes. LSM and physical emissivity techniques can be used to study how the magnitude and time scale of the associated reduction in surface emissivity, during and after precipitation events. Additionally, statistical techniques such as clustering and EOF could be used together with a before/after precipitation analysis.

We do not expect that any one of these approaches will provide a "best" estimate, rather, as a result of these analyses, we hope to have a better description of the emissivity variability under a wide variety of conditions, and this will in turn offer GPM precipitation algorithm developers a "game plan" in which to develop retrieval strategies over the next five years. Ultimately, the best measure of surface properties can be obtained from a synergistic use of passive and active microwave sensors such as the GPM GMI and DPR; however, with the majority of data coming from the GPM constellation radiometers, stand-alone techniques such as those described in this paper are still needed.

REFERENCES

[1] E. Njoku and D. Entekhabi, "Passive microwave remote sensing of soil moisture," *J. Hydrol.*, vol. 184, no. 1/2, pp. 101–129, Oct. 1996.

[2] N. Wang, C. Liu, R. Ferraro, D. Wolff, E. Zipser, and C. Kummerow, "The TRMM 2A12 land precipitation product—Status and future plans," *J. Meteorol. Soc. Jpn.*, vol. 87A, pp. 237–253, 2009.

[3] K. Gopolan, N. Y. Wang, C. Liu, and R. Ferraro, "Version 7 of the TRMM 2A12 land precipitation algorithm," *J. Atmos. Ocean. Technol.*, vol. 27, pp. 1343–1354, 2010.

[4] L. Li, P. W. Gaiser, B. C. Gao, R. M. Bevilacqua, T. J. Jackson, E. G. Njoku, C. Rüdiger, J.-C. Calvet, and R. Bindlish, "WindSat global soil moisture algorithm and validation," *IEEE Trans. Geosci. Remote Sens.*, vol. 48, no. 5, pp. 2224–2241, May 2010.

[5] W. B. Rossow and R. A. Schiffer, "Advances in understanding clouds from ISCCP," *Bull. Amer. Meteorol. Soc.*, vol. 80, no. 11, pp. 2261–2288, 1999.

[6] F. J. Turk, G. Mostovoy, and V. Anantharaj, "Soil moisture sensitivity to NRL-blend high resolution precipitation products: Analysis of simulations with two land surface models," *IEEE J. Sel. Topics Appl. Earth Observ. Remote Sens.*, vol. 3, no. 1, pp. 32–48, Mar. 2010.

[7] J. Janowiak, V. E. Kousky, and R. J. Joyce, "Diurnal cycle of precipitation determined from the CMORPH high spatial and temporal resolution global precipitation analyses," *J. Geophys. Res.*, vol. 110, no. D23, pp. D23105-1–D23105-18, 2005. doi:10.1029/2005JD006156.

[8] G. J. Huffman, R. F. Adler, D. T. Bolvin, G. Gu, E. J. Nelkin, K. P. Bowman, Y. Hong, E. F. Stocker, and D. B. Wolff, "The TRMM multi-satellite precipitation analysis: Quasi-global, multi-year, combined-sensor precipitation estimates at fine scale," *J. Hydrometeorol.*, vol. 8, no. 1, pp. 38–55, Feb. 2007.

[9] F. J. Turk and S. D. Miller, "Toward improving estimates of remotely-sensed precipitation with MODIS/AMSR-E blended data techniques," *IEEE Trans. Geosci. Remote Sens.*, vol. 43, no. 5, pp. 1059–1069, May 2005.

[10] C. Matzler, "On the determination of surface emissivity from satellite observations," *IEEE Geosci. Remote Sens. Lett.*, vol. 2, no. 2, pp. 160–163, Apr. 2005.

[11] C. Prigent, P. Aires, and W. B. Rossow, "Land surface microwave emissivities over the globe for a decade," *Bull. Amer. Meteorol. Soc.*, vol. 87, no. 11, pp. 1573–1584, 2006.

[12] C. Prigent, J. Munier, B. Thomas, and G. Ruffie, "Microwave signatures over carbonate sedimentary platforms in arid areas: Potential geological applications of passive microwave observations?" *Geophys. Res. Lett.*, vol. 32, no. 23, pp. L23405-1–L23405-4, 2005. doi:10.1029/2005GL024691.

[13] C. Prigent, E. Jaumouillé, F. Chévalliér, and F. Aires, "A parameterization of the microwave land surface emissivity between 19 and 100 GHz anchored to satellite-derived estimates," *IEEE Trans. Geosci. Remote Sens.*, vol. 46, no. 2, pp. 344–352, Feb. 2008.

[14] C. Prigent, W. B. Rossow, and E. Matthews, "Microwave land surface emissivities estimated from SSM/I observations," *J. Geophys. Res.*, vol. 102, no. D18, pp. 21 867–21 890, 1997.

[15] F. Karbou, C. Prigent, L. Eymard, and J. Pardo, "Microwave land emissivity calculations using AMSU-A and AMSU-B measurements," *IEEE Trans. Geosci. Remote Sens.*, vol. 43, no. 5, pp. 948–959, May 2005.

[16] E. Kalnay, M. Kanamitsu, R. Kistler, W. Collins, D. Deaven, L. Gandin, M. Iredell, S. Saha, G. White, J. Woollen, Y. Zhu, A. Leetmaa, R. Reynolds, M. Chelliah, W. Ebisuzaki, W. Higgins, J. Janowiak, K. C. Mo, C. Ropelewski, J. Wang, R. Jenne, and D. Joseph, "The NCEP/NCAR 40-year reanalysis project," *Bull. Amer. Meteorol. Soc.*, vol. 77, no. 3, pp. 437–471, Mar. 1996.

[17] F. Aires, C. Prigent, W. B. Rossow, and M. Rothstein, "A new neural network approach including first-guess for retrieval of atmospheric water vapor, cloud liquid water path, surface temperature and emissivities over land from satellite microwave observations," *J. Geophys. Res.*, vol. 106, no. D14, pp. 14 887–14 907, 2001.

[18] F. Aires, C. Prigent, F. Bernardo, C. Jimenez, R. Saunders, and P. Brunel, "A tool to estimate land surface emissivities at microwaves frequencies (TELSEM) for use in numerical weather prediction schemes," *Q. J. R. Meteorol. Soc.*, vol. 137, pp. 690–699, Apr. 2011.

[19] A. Jones and T. H. Vonder Haar, "Retrieval of microwave surface emittance over land using coincident microwave and infrared satellite measurements," *J. Geophys. Res.*, vol. 102, no. D12, pp. 13 609–13 626, Jun. 1997.

[20] F. Karbou and C. Prigent, "Calculation of microwave land surface emissivities from satellite observations: Validity of the specular approximation over snow-free surfaces?" *IEEE Geosci. Remote Sens. Lett.*, vol. 2, no. 3, pp. 311–314, Jul. 2005.

[21] S. Guedj, F. Karbou, F. Rabier, and A. Bouchard, "Microwave land emissivity over Antarctica: Impact of the surface approximation," *IEEE Trans. Geosci. Remote Sens.*, vol. 48, no. 4, pp. 1976–1985, Apr. 2010.

[22] F. Karbou, E. Gérard, and F. Rabier, "Global 4D-Var assimilation and forecast experiments using AMSU observations over land. Part-I: Impact of various land surface emissivity parameterizations," *Weather Forecast.*, vol. 25, pp. 5–19, 2010.

[23] F. Karbou, F. Rabier, J.-P. Lafore, J.-L. Redelsperger, and O. Bock, "Global 4D-Var assimilation and forecast experiments using AMSU observations over land. Part II: Impact of assimilating surface sensitive channels on the African Monsoon during AMMA," *Weather Forecast.*, vol. 25, pp. 20–36, 2010.

[24] B. Krzeminski, N. Bormann, F. Karbou, and P. Bauer, "Improved use of surface-sensitive microwave radiances at ECMWF," in *Proc. EUMETSAT Meteorol. Satell. Conf.*, Bath, U.K., Sep. 21–25, 2009.

[25] E. Gérard, F. Karbou, and F. Rabier, "Potential use of surface sensitive microwave observations over land in numerical weather prediction," *IEEE Trans. Geosci. Remote Sens.*, vol. 49, no. 4, pp. 1251–1262, Apr. 2011.

[26] P. W. Rosenkranz, "Water vapor continuum absorption: A comparison of measurements and models," *Radio Sci.*, vol. 33, pp. 919–928, 1998.

[27] S. V. Kumar, C. D. Peters-Lidard, Y. Tian, J. Geiger, P. R. Houser, S. Olden, L. Lighty, J. L. Eastman, P. Dirmeyer, B. Doty, J. Adams, E. Wood, and J. Sheffield, "LIS—An interoperable framework for high resolution land surface modeling," *Environ. Model. Softw.*, vol. 21, pp. 1402–1415, 2006.

[28] M. B. Ek, K. E. Mitchell, Y. Lin, E. Rogers, P. Grunmann, V. Koren, G. Gayno, and J. D. Tarpley, "Implementation of Noah land-surface model advances in the NCEP operational mesoscale Eta model," *J. Geophys. Res.*, vol. 108, no. D22, p. 8851, 2003. doi:10.1029/2002JD003296.

[29] F. Weng, B. Yan, and N. Grody, "A microwave land emissivity model," *J. Geophys. Res.*, vol. 106, no. D17, pp. 20115–20123, 2001.

[30] B. Yan and F. Weng, "Retrieval of snow surface microwave emissivity from Advanced Microwave Sounding Unit (AMSU)," *J. Geophys. Res.*, vol. 113, pp. 19206–19228, 2008.

[31] S.-A. Boukabara, K. Garrett, W. Chen, F. Iturbide-Sanchez, C. Grassotti, C. Kongoli, R. Chen, Q. Liu, B. Yan, F. Weng, R. Ferraro, T. Kleespies, and H. Meng, "MiRS: An all-weather 1DVAR satellite data assimilation and retrieval system," *IEEE Trans. Geosci. Remote Sens.*, vol. 49, no. 9, pp. 3249–3272, Sep. 2011.

[32] E. G. Njoku and L. Li, "Retrieval of land surface parameters using passive microwave measurements at 6–18 GHz," *IEEE Trans. Geosci. Remote Sens.*, vol. 37, no. 1, pp. 79–93, Jan. 1999.

[33] M. C. Dobson, F. T. Ulaby, M. T. Hallikainen, and M. A. El-Reyes, "Microwave dielectric behavior of wet soil—Part II: Dielectric mixing models," *IEEE Trans. Geosci. Remote Sens.*, vol. GE-23, no. 1, pp. 35–46, Jan. 1985.

[34] J. R. Wang and B. J. Choudhury, "Remote sensing of soil moisture content over bare field at 1.4 GHz frequency," *J. Geophys. Res.*, vol. 86, no. C6, pp. 5277–5282, Jun. 1981.

[35] E. G. Njoku and S. K. Chan, "Vegetation and surface roughness effects on AMSR-E land observations," *Remote Sens. Environ.*, vol. 100, no. 2, pp. 190–199, Jan. 2006.

[36] L. A. Jones, C. R. Ferguson, J. S. Kimball, K. Zhang, S. Chen, K. McDonald, E. Njoku, and E. Wood, "Satellite microwave remote sensing of daily land surface air temperature minima and maxima from AMSR-E," *IEEE J. Sel. Topics Appl. Earth Observ. Remote Sens.*, vol. 3, no. 1, pp. 111–123, Mar. 2010.

[37] G. Hullin, R. Fu, R. E. Dickinson, and R. Juarez, "A practical method for retrieving land surface temperature from AMSR-E over the Amazon Forest," *IEEE Trans. Geosci. Remote Sens.*, vol. 46, no. 1, pp. 193–199, Jan. 2008.

[38] X. Dong, B. Xi, and P. Minnis, "Observational evidence of changes in water vapor, clouds, and radiation at the ARM SGP site," *Geophys. Res. Lett.*, vol. 33, pp. L19818-1–L19818-4, 2006.

[39] G. Skofronick-Jackson and B. Johnson, "Surface and atmospheric contributions to passive microwave brightness temperatures for falling snow events," *J. Geophys. Res.*, vol. 116, pp. D02213-1–D02213-16, Jan. 2011. doi:10.1029/2010JD014438.

[40] F. M. Ralph, R. M. Rauber, B. F. Jewett, D. E. Kingsmill, P. Pisano, P. Pugner, R. M. Rasmussen, D. W. Reynolds, T. W. Schlatter, R. E. Stewart, and J. S. Waldstreicher, "Improving short term (0–48 h) cool season quantitative precipitation forecasting: Recommendations from a USWRP workshop," *Bull. Amer. Meteorol. Soc.*, vol. 86, no. 11, pp. 1619–1632, Nov. 2005.

[41] W. A. Peterson, D. Hudak, V. N. Bringi, P. Siqueira, A. Tokay, V. Chandrasekar, L. F. Bliven, R. Cifelli, T. Lang, S. Rutledge, and G. Skofronick-Jackson, "NASA GPM/PMM participation in the Canadian CloudSat/CALIPSO validation project C3VP. Physical process studies in Snow," in *Proc. 33rd Int. Conf. Radar Meteorol., Amer. Meteorol. Soc.*, Cairns, Australia, 2007.

[42] C. Prigent, E. Jaumouille, F. Chevallier, and F. Aires, "A parameterization of microwave land surface emissivity between 19 and 100 GHz, anchored to satellite derived estimates," *IEEE Trans. Geosci. Remote Sens.*, vol. 46, no. 2, pp. 344–352, Feb. 2008.

[43] B. Ruston, F. Weng, and B. Yan, "Use of a one-dimensional variational retrieval to diagnose estimates of infrared and microwave surface emissivity over land for ATOVS sounding instruments," *IEEE Trans. Geosci. Remote Sens.*, vol. 46, no. 2, pp. 393–402, Feb. 2008.

[44] G. Skofronick-Jackson, M.-J. Kim, J. A. Weinman, and D.-E. Chang, "A physical model to determine snowfall over land by microwave radiometry," *IEEE Trans. Geosci. Remote Sens.*, vol. 42, no. 5, pp. 1047–1058, May 2004.

[45] E. Ebert, J. Janowiak, and C. Kidd, "Comparison of near-real-time precipitation estimates from satellite observations and numerical models," *Bull. Amer. Meteorol. Soc.*, vol. 88, no. 1, pp. 47–64, Jan. 2007.

[46] C. Kidd, R. Ferraro, and V. Levizzani, "The fourth international precipitation working group workshop," *Bull. Amer. Meteorol. Soc.*, vol. 91, no. 8, pp. 1095–1099, Aug. 2010.

Ralph R. Ferraro received the B.S. degree in meteorology from Rutgers University, New Brunswick, NJ, in 1980, and the M.S. degree in meteorology from the University of Maryland, College Park, in 1982.

Currently, he is a Physical Scientist with the National Environmental Satellite Data and Information Service, National Oceanic and Atmospheric Administration, College Park, MD, where he is currently the Chief of the Satellite Climate Studies Branch. His research activities include the development of advanced retrieval algorithms for hydrological products with passive microwave sensors.

Mr. Ferraro is also a Member of the American Meteorological Society, American Geophysical Union, and the National Weather Association.

Christa D. Peters-Lidard graduated summa cum laude with the B.S. degree in geophysics and a minor in mathematics from Virginia Polytechnic Institute and State University (Virginia Tech), Blacksburg, in 1991, and the M.A. and Ph.D. degrees from the Water Resources Program in the Department of Civil Engineering and Operations Research, Princeton University, Princeton, NJ, in 1993 and 1997, respectively.

Currently, she is the Chief of the Hydrological Sciences Laboratory at NASA's Goddard Space Flight Center, Greenbelt, MD, where she has been a Physical Scientist since 2001. Currently, she is the Chief Editor for the American Meteorological Society (AMS) *Journal of Hydrometeorology* and an elected Member of the AMS Council and was elected as an AMS Fellow in 2012. Her research interests include land-atmosphere interactions, soil moisture measurement and modeling, and the application of high performance computing and communications technologies in earth system modeling, for which her Land Information System team was awarded the 2005 NASA Software of the Year Award.

Cecilia Hernandez received the B.S. and M.E. degrees in civil engineering from the University of Puerto Rico, Mayaguez, in 2001 and 2007, and the M.Phil. degree in civil engineering from the City College, the City University of New York, in 2009. She received the Alfred P. Sloan Foundation Graduate Scholarship at the City College of New York as well as a NOAA-CREST Fellowship.

Since 2010, she has been a Faculty Research Assistant at the University of Maryland, College Park, where she performs research in the areas of passive microwave remote sensing of precipitation and surface parameters.

F. Joseph (Joe) Turk received the B.S. and M.S. degrees in electrical engineering from Michigan Technological University, Houghton, in 1982 and 1984, respectively, and the Ph.D. degree in electrical engineering (specialization in microwave remote sensing) from Colorado State University, Fort Collins, in 1992.

From 1995 to 2008, he was affiliated with the Naval Research Laboratory, Monterey, CA. Currently, he is with the Radar Science group at the Jet Propulsion Laboratory, Pasadena, CA. His current research interests are in microwave radar and radiative transfer modeling of clouds, precipitation, and land surfaces; aircraft and satellite analysis of cloud properties and inversion techniques; and validation of satellite-based precipitation data sets.

Filipe Aires received the Ph.D. degree in statistics from the University Paris-Dauphine, Paris, France, in 1999.

He was with the NASA Goddard Institute for Space Studies, New York, for five years as a Postdoc and Research Scientist. He then obtained a Centre National de la Recherche Scientifique Research Scientist Position at the Laboratoire de Météorologie Dynamique, Paris, France. His research interests focus on satellite remote sensing of the earth and statistical analysis of the climate. In earlier works, he analyzed climatic signals such as El Nino, using statistical techniques such as independent component analysis. He specializes in the exploitation of the multiwavelength synergy. Recently, he has developed for CNES, the French spatial agency, the SAPHIR/MADRAS water vapor algorithms for the French-Indian mission Megha-Tropiques launched in 2011. Presently, he is involved in various studies linked to the retrieval of infrared and microwave surface emissivities and atmospheric retrievals over land such as Global Precipitation Mission. He is developing a long-term global soil moisture data set based on multiwavelength satellite observations. He is the Cofounder and Chief Executive Officer of Estellus, a startup in the domain of remote sensing and climate impacts.

Catherine Prigent received the Ph.D. degree in physics from Paris University, Paris, France, in 1988.

Since 1990, she has been a Researcher with the Laboratoire d'Etudes du Rayonnement et de la Matière en Astrophysique, Paris Observatory, Centre National de la Recherche Scientifique (CNRS), Paris, France. From 1995 to 2000, she was on leave from CNRS and worked at the NASA Goddard Institute for Space Studies, Columbia University, New York, NY. Her research interests focus on passive microwave remote sensing of the earth. Her early work focused on the modeling of the sea surface emissivities at microwave wavelengths and the estimation of atmospheric parameters over the ocean from microwave measurements. Currently, her main interests include the calculation and analysis of microwave land surface emissivities, estimation of atmospheric and surface parameters over land from microwave observations, as well as multisatellite characterization of the land surface. She is also involved in satellite remote sensing of clouds with the analysis of passive microwave observations over convective cloud structures.

Xin Lin received the M.S. and Ph.D. degrees from Colorado State University, Fort Collins, in 1992 and 1997, respectively.

Currently, he is a Research Scientist in the Earth System Science Interdisciplinary Center, University of Maryland College Park/NASA Goddard Space Flight Center. His primary research interests include satellite precipitation retrieval evaluation and data assimilation, rain intensity, and frequency estimations associated with climate changes.

Sid-Ahmed Boukabara received the Engineer and M.Sc. degrees in signal processing from the National School of Civil Aviation, Toulouse, France, and from the Institut National Polytechnique de Toulouse, France, respectively, both in 1994. He received the Ph.D. degree in remote sensing from the Denis Diderot University, Paris, France, in 1997.

He was then involved in the calibration/validation of the European Space Agency's European Remote Sensing-2 microwave radiometer and has worked on the synergistic use of active and passive microwave measurements. He then joined AER Inc. in Cambridge, MA, as a Staff Scientist and worked on the design, implementation, and validation of the National Polar-orbiting Operational Environmental Satellite System/Conical-scanning Microwave Imager/Sounder physical retrieval algorithm, on the NASA SeaWinds/QuikSCAT wind vector rain flag and on the development of the atmospheric absorption model MonoRTM, dedicated to the microwave and laser applications. In 2005, he joined NOAA/NESDIS in Camp Springs, Maryland, and is leading an effort to develop the capability of assimilating passive microwave measurements in all-weather conditions using a combination of variational technique algorithm and the community radiative transfer model. Since 2009, he also serves as the Deputy Director of the U.S. Joint Center for Satellite Data Assimilation. His principal areas of interest include radiative transfer modeling, spectroscopy, algorithm development, and satellite data assimilation.

Fumie A. Furuzawa received the Ph.D. degree in astrophysics from Nagoya University, Nagoya, Japan, in 2000. Since 2002, she has been studying land rainfall observed with Tropical Rainfall Measuring Mission at Hydrospheric Atmospheric Research Center of the Nagoya University.

Currently, she is working on the development of a land surface microwave emissivity algorithm with satellite measurements in order to improve rain retrieval for the development of radar-radiometer combined algorithm as part of Japan Aerospace Exploration Agency Global Precipitation Measurement Mission projects.

Kaushik Gopalan received the B.E. degree in electronics and communication from the Rashtreeya Vidyalaya College of Engineering, Bangalore, India, in 2003, and the M.S. and Ph.D. degrees in electrical engineering from the University of Central Florida, Orlando, in 2005 and 2008, respectively.

Currently, he is employed at the Space Applications Center, Ahmedabad, India, where he works on geophysical retrievals from passive microwave sensors.

Kenneth W. (Ken) Harrison received the Ph.D. degree in civil engineering from North Carolina State University (NCSU), Raleigh, in 2002.

He conducts research in environmental and water resources systems analysis at NCSU. His primary research area is decision-making under uncertainty. Of secondary interest is the accounting of uncertainty in modeling via Bayesian methods, the development of computationally based decision support tools, and the optimization of large-scale systems. Applications extend from the adaptive management of water quality, water distribution systems modeling, water quantity management, assessment of the external damages of power generation, integrated solid waste management, and energy modeling. Most recently, he helped to develop extensions in the NASA Land Information System to carry out uncertainty estimation via Markov chain Monte Carlo methods for Bayesian analysis for application to land surface and land surface-coupled models including microwave emissivity models.

Fatima Karbou received the B.S. degree in topography from the Institut Agronomique et Vétérinaire Hassan II, Rabat, Morocco, in 1999, and the Ph.D. degree in physics of remote sensing from Versailles Saint-Quentin-en-Yvelines University, Versailles, France, in 2004.

Since January 2007, she has been with the National Center for Meteorological Research/GAME, Météo-France, France, as a Researcher with Ministère de l'Ecologie, du Développement Durable, des Transports et du Logement. She is an expert in passive microwave remote sensing, radiative transfer modeling, and data assimilation. Her current main research activity is the assimilation of cloudy/rainy microwave observations over land surfaces. Her research topics also include inverse problems over complex surfaces such as snowpack/sea ice with a particular interest in modeling the emissivity of these complex surfaces.

Li Li (M'96–SM'06) received the Ph.D. degree in electrical engineering from the University of Washington, Seattle, in 1995.

Currently, he is with the Naval Research Laboratory, Washington, DC. His primary interests are in the passive and active microwave remote sensing of soil moisture, vegetation, snow, and precipitation for climate applications. He is the Land Algorithm Lead for the WindSat instrument and a Member of the DoD Soil Moisture Applications Consortium. From 1997 to 2004, he was a Senior Scientist at the Jet Propulsion Laboratory, California Institute of Technology. From 1995 to 1997, he was with the Caelum Research Corporation, working at NOAA/NESDIS Office of Research and Application, Camp Springs, MD.

Dr. Li is a Member of the American Geophysical Union. He has been a recipient of the IEEE Geoscience and Remote Sensing Society Transactions Prize Paper Award 2009, NASA Group Achievement Awards in 2002 and 2008, JPL Technical Excellence Award in 2002, and NCAR/RAP fellowship 1993–1995.

Chuntao Liu received the Ph.D. degree in atmospheric science from the University of Wyoming, Laramie, in 2003.

Currently, he is a Research Associate Professor with the Department of Atmospheric Sciences, University of Utah. His research interests include the ground-and satellite-based remote sensing, clouds and precipitation, and extreme events. He takes the lead on developing the event-based database from Tropical Rainfall Measuring Mission observations and is author/coauthor of 30 peer-reviewed publications.

Hirohiko Masunaga received the Ph.D. degree in astrophysics from University of Tokyo, Tokyo, Japan, in 1999.

He has since been engaged primarily in satellite data analyses with focus on tropical meteorology and climatology including convectively coupled equatorial waves and moist convective dynamics. He is involved in the Global Precipitation Measurement as a Principal Investigator of the Japan Aerospace Exploration Agency Precipitation Measuring Mission. Currently, he is currently Associate Professor at Nagoya University, Japan.

Leslie Moy received the M.S. degree in meteorology from the University of Maryland, College Park, in 1992.

Recently, she joined I.M. Systems Group at NOAA/NESDIS, Camp Springs, MD, as a Support Scientist. Her current effort is focused on integrating the Global Precipitation Measurement Mission's Microwave Imager into the Microwave Integrated Retrieval System.

Sarah Ringerud received the B.S. degree in atmospheric and oceanic sciences and mathematics from the University of Wisconsin-Madison, in 2002, and the M.S. degree in Atmospheric Science from Colorado State University, Fort Collins, in 2006.

Currently, she is working toward the Ph.D. degree in Atmospheric Science at Colorado State, focusing on passive microwave remote sensing over land surfaces.

Gail M. Skofronick-Jackson received the B.S. degree in electrical engineering from Florida State University, Tallahassee, and the M.S.E.E. and Ph.D. degrees from the Georgia Institute of Technology, Atlanta.

In 1997, she began working at NASA Goddard Space Flight Center in Greenbelt, MD as a Postdoctoral Research Associate. Currently, she is a Government Physical Scientist at NASA in the Mesoscale Processes Branch. She is Deputy Project Scientist for the Global Precipitation Measurement mission. Her research interests include using satellite remote sensing to estimate rain rate, snowfall rate, and the vertical profiles of clouds.

Dr. Skofronick-Jackson is also a Member of the American Meteorological Society and the American Geophysical Union.

Yudong Tian received the Ph.D. degree in atmospheric sciences from the University of California at Los Angeles (UCLA), Los Angeles, in 1999.

He conducted research in climate dynamics and geophysical fluid dynamics at UCLA. He was also one of the developers at UCLA for the popular Advanced Spectral Analysis SSA-MTM Toolkit. Between 2000 and 2002, he had been working in the Internet industry, holding such positions as Systems Manager and Chief Technology Officer. He started to work for the NASA Goddard Space Flight Center, Greenbelt, MD, in 2002, first on the development of the Land Information System, which won NASA's Software of the Year Award in 2005. More recently, he has been evaluating and validating satellite-based precipitation measurements and also working on land surface emissivity modeling to support NASA's Global Precipitation Measurement mission.

Nai-Yu Wang received the B.S. degree in meteorology from Chinese Culture University, Taipei, Taiwan, in 1987, and the M.S. and Ph.D. degrees in atmospheric sciences and remote sensing from the University of Michigan, in 1993 and 1998, respectively.

Currently, she is an Assistant Research Engineer in the Earth System Science Interdisciplinary Center, University of Maryland, College Park, where her work focuses on satellite remote sensing of precipitation, including forward model development and inversion techniques from microwave, infrared, and lightning sensors.